NMR Studies of the T_{1z} Relaxation Times of the PMSN Ferroelectric

A thesis submitted in partial fulfillment of requirements for the degree in Bachelor of Science in Physics from The College of William and Mary in Virginia

by

Joseph P. Palamara

Accept for: BS with Honors in Physics _____

_____

Advisor: Dr. Gina Hoatson

_____

Dr. Robert Vold

_____

Dr. Charles Perdrisat

_____

Dr. Todd Averett

Williamsburg, VA

April, 2011

Abstract

^{93}Nb MAS studies in the solid solution Lead Magnesium Scandium Niobate (*x*PMSN): $(1-x)Pb(Mg_{1/3}Nb_{2/3})O_3-xPb(Sc_{1/2}Nb_{1/2})O_3$ have been performed to probe the microscopic nature of relaxor ferroelectricity. Using the *x*=0.6 concentration of PMSN, saturation recovery pulse sequence experiments were performed at various temperatures to study the longitudinal relaxation times in the system. A series of both one dimensional and two dimensional experiments were used to probe the system to determine specific features, in particular relaxation times T_{1z}.

Using the one dimensional single quantum experiments, the four largest peaks in the spectrum were analyzed, and it was seen that there is little temperature dependence in the frequencies of the peaks, but significant temperature dependence in their relaxation times T_{1z}. Looking at these temperature dependences allows us to conclude that the relaxor behavior is significantly dependent on the local dynamics of the ions in the crystal units.

The two dimensional triple quantum MAS experiments were performed in an attempt to improve spectral resolution, allowing us to look at the behavior of a wider peak that could not be clearly resolved in 1D spectral analysis. With the decreased signal to noise in the 2D spectra, only two peaks could be analyzed with statistical confidence. However, it was seen that these peaks were significantly separated and longer and more accurate relaxation times were obtained at 300 Kelvin.

List of Figures

Contents

1 Theory

1.1 NMR Theory

Nuclear Magnetic Resonance (NMR) is one of many tools used to examine the microscopic structure and dynamical properties of substances of interest. Every atom has a nucleus comprised of protons and neutrons. Most nuclei have spin in addition to charge. As with any moving charge, a magnetic moment is associated with the nucleus. By examining the response of nuclear magnetization to external and local magnetic fields, molecular structure and dynamics can be studied.

1.1.1 Quantum Mechanical Theory

To fully understand how NMR works, we need to use quantum mechanics and perturbation theory. When placed in a strong magnetic field, a spinning nucleus experiences the Zeeman Effect, where the Hamiltonian is defined by $H_z = -\mu \cdot B$, where B is the applied magnetic field (generally defining the z-axis) and μ is the magnetic moment of the nucleus, a product of spin and gyromagnetic ratio. This Zeeman energy is associated with a frequency of precession ω_0 about the applied field, called the Larmor frequency. If a nucleus were to be perfectly isolated and examined, it would precess about the static applied field at its Larmor frequency. For example, ^{93}Nb nuclei in our 17.63 T spectrometer spin at a frequency of 183.6 MHz. When materials begin to grow more complicated and less uniform, embedded nuclei shift their resonant frequencies.

It is these more complicated materials that require perturbation theory to explain shifts in resonant frequency. Basic perturbation theory says that there is a main Hamiltonian, and small changes that add to it from smaller effects. In NMR studies, the

overall Hamiltonian is $H = H_Z + H_{perturbations}$ with the Zeeman Hamiltonian primarily defining the resonant frequency, which is then shifted slightly by the perturbations. There are a number of molecular effects that can cause these perturbations. Some of the most common in NMR are Dipole-Dipole Coupling, Isotropic Chemical Shift, and the Electric Quadrupole Shift.

Dipole-Dipole Coupling occurs when there are two or more spins in close proximity. The spinning nuclei create their own magnetic field, influencing the magnetic field felt by those nuclei near them. With this change in local magnetic field, the resonant frequencies of nuclei being studied are slightly shifted, making the Hamiltoninan $H = H_Z + H_{dipole\text{-}dipole}$, either increasing or decreasing the resonant frequency depending on the spins of neighboring nuclei and the orientation of their internuclear vectors with respect to the external field. This is an anisotropic effect meaning that the shift is dependent on orientation. There are methods that can minimize anisotropic effects (Magic Angle Spinning, which will be discussed later).

The Isotropic Chemical Shift is also due to the surrounding environment. The electron clouds surrounding the nuclei studied create additional shift in resonant frequency due to the electrons' interaction with the magnetic fields. There is both an anisotropic component (minimized by MAS), and an isotropic component (independent of orientation). In some materials, this shift can be comparable to the dipolar interaction.

The Electric Quadrupole Interaction is the most important perturbation in the material studied in this paper, the PMSN system. For nuclei with a spin value *I* greater than 1, the asymmetric distribution of charge over the nucleus can create an electric quadrupole moment. This electric quadrupole moment interacts with the local Electric

Field Gradient (EFG) produced by local charges, and further changes the resonant frequency. The symmetry of the interactions mentioned above is characterized by associated Legendre Polynomials of rank 2. The final perturbation is a sum of orders of magnitude from zero order to n^{th} order, with a higher n^{th} order leading to a more accurate approximation. However, for most perturbations, terms past 2^{nd} order are generally insignificant and ignored due to their miniscule contribution. The electric quadrupole shift actually is still significant to second order, and in fact is the most prominent perturbation in the PMSN system. In order of greatest magnitude, the overall Hamiltonian for the PMSN system is $H = H_z + H_{Q,1} + H_{Q,2} + H_{iso}^{CS}$ where H_z is the Zeeman Hamiltonian, H_Q are the Quadrupole Perturbations (first and second order), and H_{iso}^{CS} is the Isotropic Chemical Shift.[3, 4, 5]

1.1.2 Magic Angle Spinning

In static, solid state samples, the spectra of resonant frequencies create what is called a powder pattern. This is due to anisotropic effects of magnetic field and EFG tensor, which depend on the orientation of the sample. There are methods used to average these anisotropic effects and create sharper, more distinct peaks from disperse powder patterns. The most common method is to use liquid samples. In liquids, the molecules move relatively freely and this motion allows for averaging out of the anisotropic effects, and only the isotropic spectrum remains, where distinct sites can be more easily identified on the basis of chemical shifts.

Of course, not every material studied can be studied in a liquid state. When it is not possible, we use the process of Magic Angle Spinning (MAS). First, a solid sample is

ground into a fine powder then placed into a small rotor, ideally not containing any nuclei with similar Larmor frequencies. The rotor is then spun at high speeds (a few kHz for larger rotors, up to about 35 kHz for smaller rotors) at a specified angle known as the Magic Angle. At this angle, about $\theta = 54.7$ degrees from the alignment of the applied magnetic field, the term $(3\cos^2\theta-1)$ becomes zero, which nullifies second rank tensors, thereby collapsing powder patterns to a narrow center band and a series of narrow sidebands.

The magic angle must be set as precisely as possible or anisotropic effects of these second rank tensors will still be prevalent and the spectrum and eigenfrequencies will remain unresolved. In order to do this, we use a material called deuterated debacic acid/UIC (urea inclusion compound), $(DOOC)(CH_2)_8(COOD)$ where the carboxyl hydrogen atoms have been replaced by deuterons. When spinning not exactly at the magic angle, the spectrum of the sebacic acid shows significant quadrupole splitting, shown in the figure below.

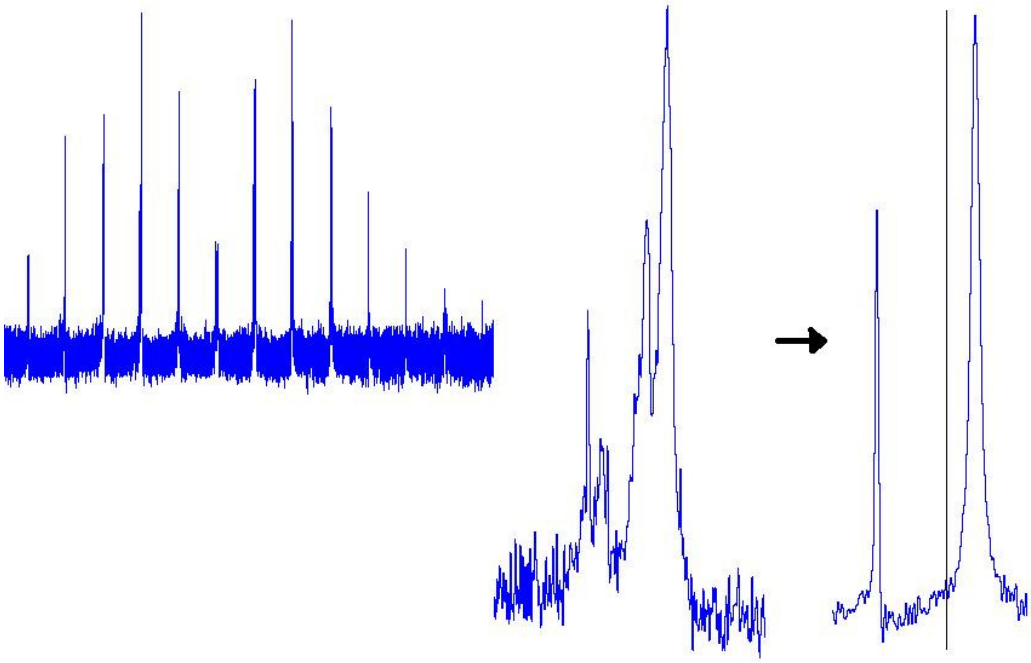

Fig 1: Spectrum of sebacic acid, zoomed in on largest band, from off MAS to on MAS

As the angle of spin is brought closer to the magic angle, the quadrupole splitting is slowly removed and the peaks join into one narrow, intense peak. Once the magic angle is set, the peaks hit their highest intensity and narrowest width, and the sebacic acid can be removed to study other materials using accurate MAS.[1, 2, 3, 4]

1.1.3 Radio Frequency NMR

In order to actually see the effects of the resonant frequencies in materials studied using NMR, we need to employ the use of radio waves to excite the spins. It is through the magnetic field of RF pulses that we can manipulate the angular momentum of nuclei. By applying a pulse at the resonant frequency of specified power and duration, the overall magnetization vector of the material being studied can be rotated. Depending on site-specific perturbations, the magnetization will take a certain time to return to its

thermal equilibrium state in alignment with the applied magnetic field. This is called relaxation, and will be discussed in the next section.

Once the spins have been pulsed, the sample may be given a certain amount of time to return to its equilibrium state. It is then hit with a pulse to rotate the magnetization ninety degrees away from the alignment of the magnetic field into the acquisition dimension (in our spectrometer, the *x*-*y* plane). It is at this point that the spectrum begins to be read. Around the rotor that the sample is packed in, there is a conducting coil. The magnetization precesses about the applied field, returning to the equilibrium state, and this precession induces a small current into the coil around the sample. The more sample is packed into the rotor, the greater signal can be achieved in a single experiment due to more nuclei contributing to the magnetization vector.

The induced current is read as a voltage, digitized, and stored in memory as a Free Induction Decay (FID), plotted as voltage vs. time. The FID is then Fourier transformed to achieve a spectrum in frequency space, centered on the Larmor frequency. The FID and associated full spectrum for the fully relaxed PMSN system at 320 K are shown below.

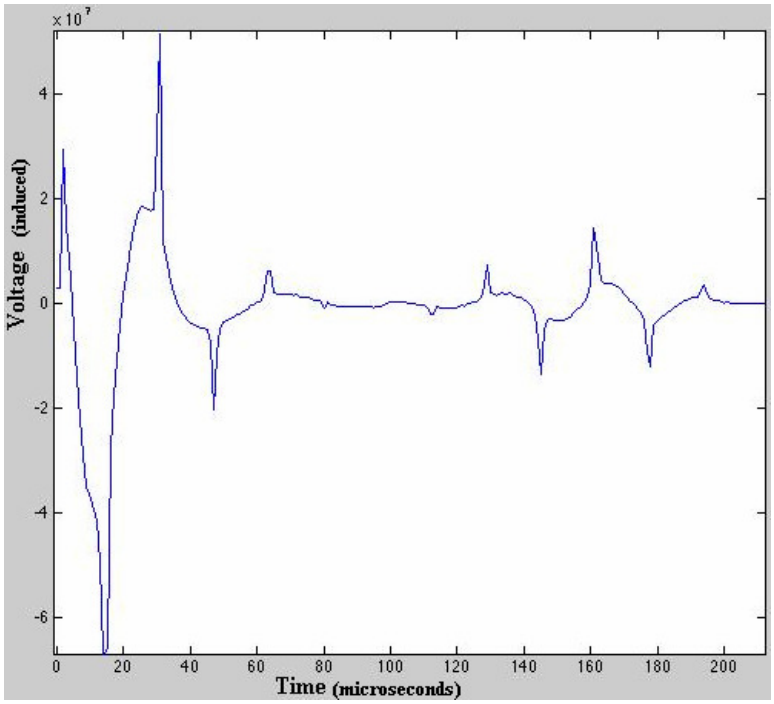

Fig 2: FID for PMSN at 320K

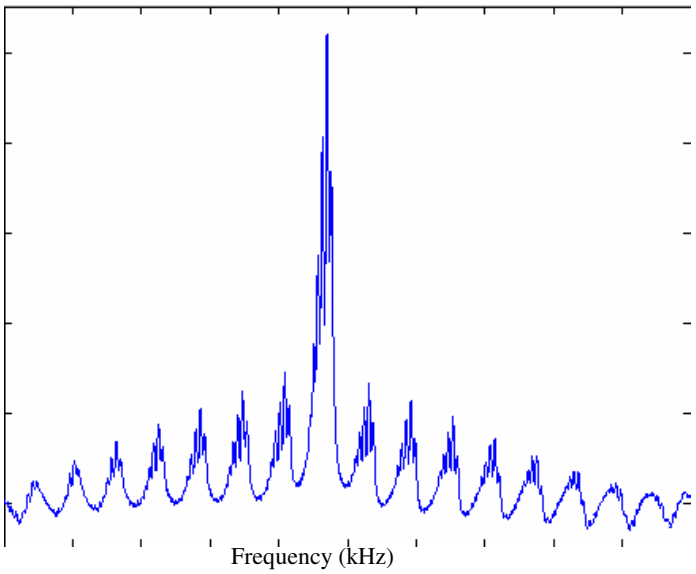

Fig 2A: full spectrum of PMSN at 320K

When acquiring a FID, careful consideration must be taken in deciding where the true signal begins. There is an effect called ringdown, in which the 90 degree pulse used

to rotate the magnetization into the acquisition dimension still hasn't quite completely faded away, and the electronics reading the induced current are still affected by it. Therefore before attempting to Fourier transform, we generally need to ignore a few of the early points in the FID, or left shift the spectrum. It is standard practice to left shift to the top of the first rotary echo. If we ignore too many points, then we begin to lose legitimate signal and valuable information, but if we use too much then we have artifact data that is not part of the true spectrum.

In the spectrum shown in Fig 2A, there is one center band with a number of smaller frequency bands on the sides that resemble the center band in shape. These are called spinning sidebands, and are separated by the spinning frequency (30 kHz in this case). They are caused by satellite transitions. In our one dimensional studies, we look primarily at the center band, in which magnetic quantum number m changes from +1/2 to -1/2. The satellite transitions also involve $|\Delta m| = 1$, but unlike the central transition are subject to first order quadrupole coupling. The center band is therefore much narrower and more intense. For electromagnetic radiation, the only 'allowed' transitions are $\Delta m = 1$, so you cannot have a jump from +1/2 to -5/2, however specific pulse programs are described later that reveal 'forbidden coherences' of any order, in particular $\Delta m = 3$. Spinning sidebands can also be used for NMR analyses, but were not used in research in this thesis.[3, 4]

1.1.4 Longitudinal Relaxation

In our studies, we use a saturation pulse train before the final acquisition pulse. This means that we barrage the sample with forty 90 degree RF pulses to completely

randomize the magnetization over a sphere. We then allow a delay for the precession to at least partially return magnetization to the z-axis in line with the applied magnetic field. The actual rate at which the magnetization returns is dependent on temperature, as well as static and dynamic properties of the system being studied. Spin Lattice Relaxation (T_{1z}) will be discussed further in section 2, the one dimensional analysis of the PMSN system.[4]

1.2 Ferroelectricity

Ferroelectric materials have become increasingly important in the last few decades. Due to their high dielectric value, they are used often in capacitors, and the hysteresis-like property of ferroelectricity makes them useful for memory and in devices such as sonar.

To understand ferroelectricity, it may be easier to draw an analogy to ferromagnetism. In ferromagnetic materials, electrons line up so that there is a net magnetization along one direction. This leads to the north/south polarization in common magnets; there is a greater number of electrons spinning along that axis. Ferroelectric materials do not have a magnetic dipole, but instead an electric dipole. When put into an electric field, most nonconducting materials display semi-linear polarization, shown in figure 3 below.

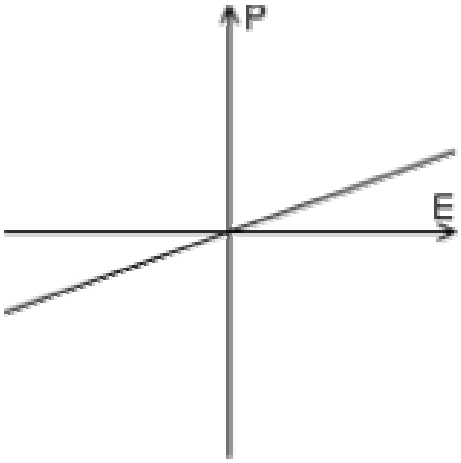

Fig 3: Linear Dielectric Polarization plot of Electric Field vs. Polarization

This is common dielectricity. The electric field pushes the positive nuclei in the opposite direction of the negative electrons, leaving a nonhomogenous charge distribution, with one side being slightly more positive and one side being slightly more negative. In the majority of materials, this polarization is proportional to the electric field they are exposed to. Linear dielectrics are mathematically the simplest displays of polarization. Paraelectric materials lose the linear proportionality, but still maintain no net dipole when removed from an electric field as shown in figure 4.

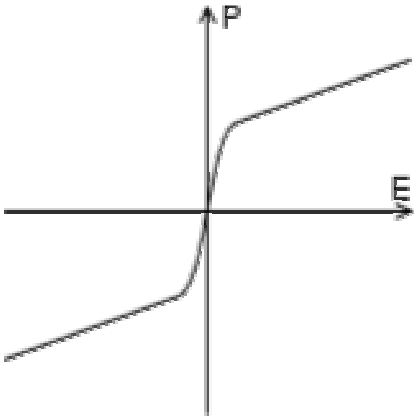

Fig 4: Paraelectric Polarization showing nonlinear response

Ferroelectric materials, after being placed in an electric field, will maintain a remnant dipole when completely removed from the field. They only display this property below a certain temperature (the Curie Temperature), near which they undergo a phase transition from para- to ferroelectric state. When in the ferroelectric state, they display a hysteresis effect in their polarization, as in figure 5, which can be used as memory.

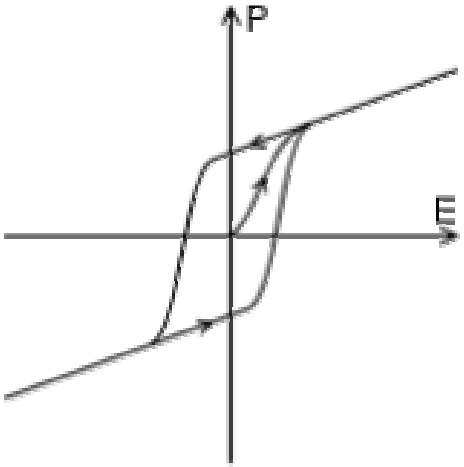

Fig 5: Ferroelectric Polarization, nonlinear with remnant polarization

Ferroelectrics often also display the extremely useful properties of piezoelectricity and pyroelectricity. Piezoelectric materials create electric dipoles when physical stress is applied, and can also change shape when a voltage is applied. This property is particularly useful in many things ranging from musical instrument pickups to microscopic piezoelectric motors. Pyroelectricity is a very similar property; pyroelectrics respond to changes in temperature the same way piezoelectrics respond to physical stress.

These properties, along with their high dielectric values, make the study of ferroelectrics an important scientific undertaking. By better understanding the microscopic nature of ferroelectricity, more powerful ferroelectric materials can be created.

A more recently discovered subclass of ferroelectrics is materials displaying relaxor ferroelectricity. While standard ferroelectrics generally have a unique transition temperature from the para- to ferroelectric state, relaxors have a broad phase transition that spans a greater temperature range. These materials also generally have more pronounced properties, particularly higher piezoelectric coefficients, which ferroelectrics are so valued for. The microscopic origin of relaxor ferroelectricity is still being studied, as we have done with the materials examined in this thesis.[3]

1.3 The PMSN System

The ferroelectrics we study belong to a class of crystals called Perovskites, crystals with the chemical form of ABO_3, with A and B representing different component sites within a unit cell of the crystals. A particularly large number of ferroelectrics are of perovskite form. A basic image of a general perovskite crystal is shown below

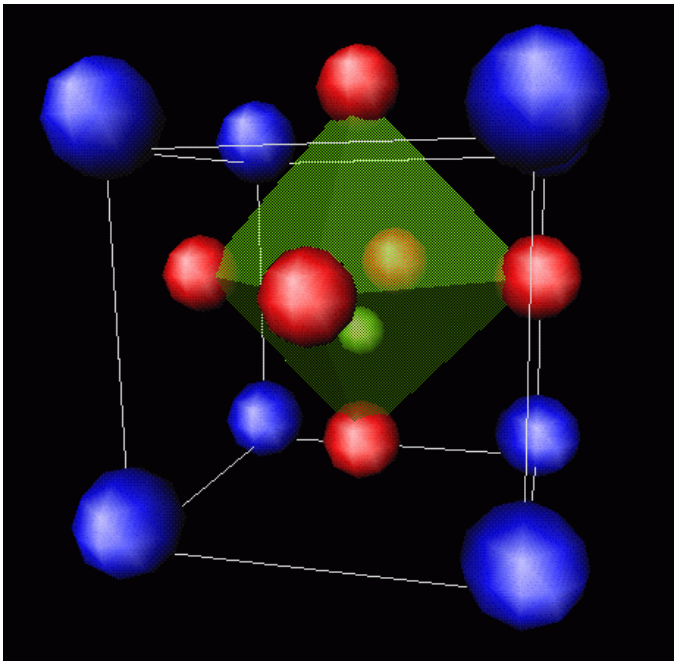

Fig 6: Perovskite structure of A site (blue), B site (green), and Oxygen (red)

The lead based relaxor systems (1-*x*)Pb($Mg_{1/3}Nb_{2/3}$)O_3:*x*Pb($Sc_{1/2}Nb_{1/2}$)O_3 or *x*PMSN solid solutions have been used for significant study in part due to their relatively low phase transition temperature (~285K)**.** By using Magic Angle Spinning (MAS), second rank spherical tensor components (involving the term $3\cos^2\theta$-1) are removed, and what would be powder patterns become much more clearly resolved, allowing for clearer insight into structure**.** Many X-ray, Electron Microscopy, and NMR studies have looked into the structure of the systems and arrived at significant conclusions of the overall lattice structure of unit cells, in particular the possible nearest B site neighbor (nBn) configurations. The accepted model has a unit cell with a B cation of $Nb^{5+,}$ $Sc^{3+,}$ or Mg^{2+} surrounded by a distorted octahedron of O^{2-} anions, Pb^{2+} ions, and a shell of the 6 nearest B site neighbor cations. There are 28 possible nBn configurations, each designated by the number of $Mg^{2+,}$ Nb^{5+}, and Sc^{3+} cations surrounding a specified B

site, written as (N_{Mg}, N_{Sc}, N_{Nb}). Each cation number can range from 0 to 6, with the total sum of all the cations constrained to 6. Figure 7 shows a diagram displaying the possible nBn configurations of a PMSN system**.** The congifurations of (N_{Mg}, 6- N_{Mg}, 0) which have no Nb^{5+} neighbors are designated peaks 0-6, based on the number of Mg^{2+} neighbors.

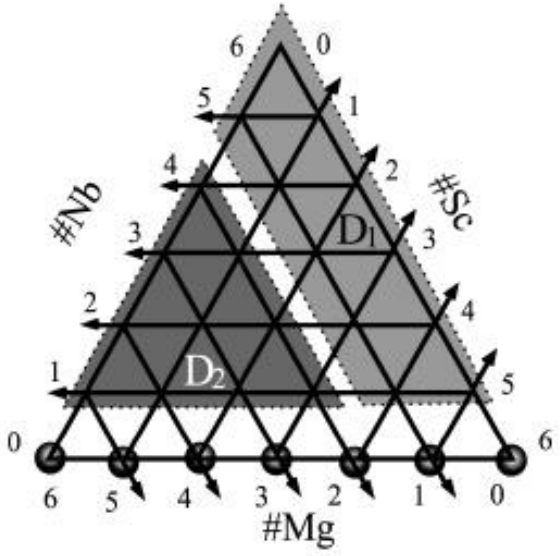

Fig 7: PMSN sites[3] of D1 and D2 distributions and narrow peaks P0-P6

Due to the similar ionic radii, electronegativities, and valences of Mg^{2+} and $Sc^{3+,}$ these configurations have relatively high symmetry and therefore smaller electric field gradients, giving rise to seven distinct peaks. However, the significant difference in properties of the Nb^{5+} nuclei leads to much greater distortion of cubic symmetry when N_{Nb} is not equal to zero, and leading to greater electric field gradients and therefore greater quadrupolar effects. These differences lead to greater linewidths, and the variety of configurations cannot be resolved, creating the broader distributions D1 and D2.

Figure 8 shows the ^{93}Nb spectrum at 320 K, with a simple deconvolution into the seven sharp peaks and the D1 peak.

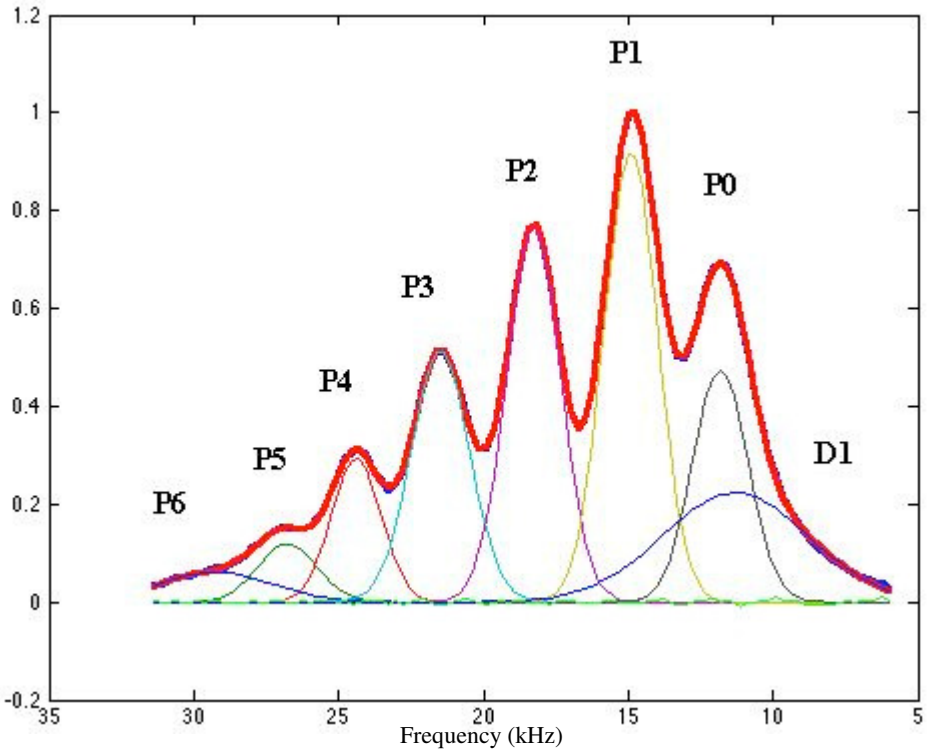

Fig 8: 93Nb spectrum of PMSN, deconvoluted into peaks

Studies into the structure of PMSN systems have revealed certain amounts of both order and disorder, depending in part on the concentration *x* of the solid solutions. For solutions other than pure PMN (*x*=0), there is a B site chemical order along the <111> direction, following what is called a "random site" model $Pb(\beta'_{1/2}\beta''_{1/2})O_3$, where β' is a random mixture $[Mg^{2+}_{2(1-x)/3}Sc^{3+}_{x}Nb^{5+}_{(1-x)/3}]$ and β" is made purely of Nb^{5+} cations, and the B site cations alternate between β' and β" along the <111> direction. It has been largely accepted that the random site disorder in the B sites leads to relaxor behavior.

However, this study looks not only at the structure of the lattice, but attempts to examine the motion of the ions in the system to see if phonon modes may account for some of the ferroelectric properties. By studying the longitudinal relaxation times (T_{1z}) of individual peaks and examining their frequency shifts, we can look into the effects of the motion of the atoms in the lattice.[1, 2, 3]

2. One Dimensional T_{1z} Analysis

2.1 Experimental Methods

This particular study looked solely at the *x*=0.6 concentration of PMSN, which was provided by Dr. Peter Davies of the University of Pennsylvania, and has been thermally annealed to better than 95%. They have been examined in detail with MAS experiments by D. Zhou, M. Vijayakumar, R. Vold, G. Hoatson, and others, as well as having been investigated by x-ray diffraction, transmission electron microscopy, and dielectric measurements. Multiple Quantum Coherence MAS experiments have been used with significant success in studying the crystalline structure, but for this part of our study we used a simple single quantum experiment to study the relaxation times of individual peaks.[1, 2, 3] The particular pulse sequence used is the saturation recovery sequence, in which a chain of 90 degree pulses is applied to the spinning sample with little time to allow the sample to recover, leaving it in a saturated state throughout the chain. There is then a variable delay applied to examine the relaxation before another final 90 degree pulse, after which the FID is digitized and processed.

For this study, the pulse program, shown below, was optimized to a 90 degree pulse of strength 3 dB for 1.6 microseconds. In the saturation pulse train, the delay between pulses was 50 microseconds. For the variable delay before the final 90 degree pulse, we used values from 50 microseconds to 100 milliseconds, at least twice the longest possible expected relaxation time for any peak, making sure to allow the spin system to fully relax. Due to the relatively close resonant frequency of the Scandium nuclei, we needed to use a more selective pulse to remove overlap of Scandium resonance.

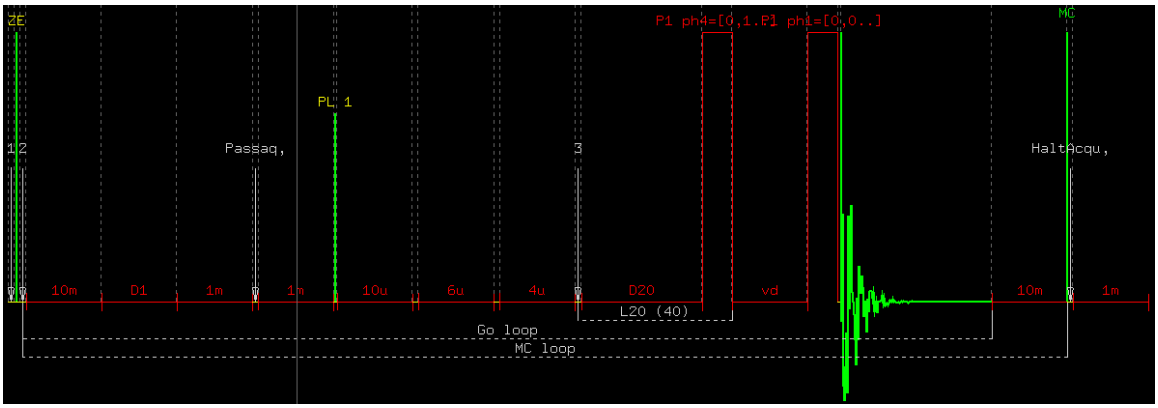

Fig 9: 1D Pulse Program as shown in Topspin with saturation train and 90 degree pulse

We performed the experiment at a number of temperatures from 230 K to 320K while spinning at 30 kHz, generally within +/- 4 Hz, while temperature was calibrated to within +/- 0.1 K. The temperatures stated in this study are set point temperatures, not necessarily the true sample temperature. Previous studies have shown that while spinning at 30 kHz, the true temperature is about 30 K higher than the set point, but this must be calibrated carefully. The PMSN sample was spun in a 2.5 mm rotor in a field of 17.6 T. We used 2048 scans for each variable delay, and examined the spectrum in a window of

500 kHz centered at 183.6 MHz. In order to significantly increase the signal-to-noise ratio, we applied a band pass filter to only allow frequencies from 120 to 205 MHz, then an additional 20 MHz band pass filter to allow only frequencies from 178-198 MHz.

We used a Bruker Avance NMR spectrometer along with Topspin 2 to control experiments, temperature, and spinning rate. To process the data, we used a MATLAB program made by R. Vold called NMRLV capable of left shift, phasing, curve fitting, and a number of other utilities necessary for NMR study. In the processing, we used 1x zero fill to improve resolution, and did not use line broadening (neither of which improves S/N).

2.2 Results and Analysis

When processing the spectra, we first noted that linewidths seemed to have become much clearer in this study than they have been previously, even though the exact same sample had been used. To display the overall range of resolution for this study, figure 10 displays the center spectrum at the lowest temperature studied, 230 K. Note that resolution and linewidths depend on the temperature: at higher temperatures, lines are narrower and resolution becomes much better. At the lowest temperature studied, only the frequencies of peaks 0 through 3 can be identified with significant certainty. It is not until we reach a temperature of 270 K that we can reliably identify the frequencies of peaks 0 through 5 (peak 6 cannot be identified as it is only a small tail past the other peaks, while peak D1 resides beneath the rest of the spectrum, usually around peak 0 or peak 1).

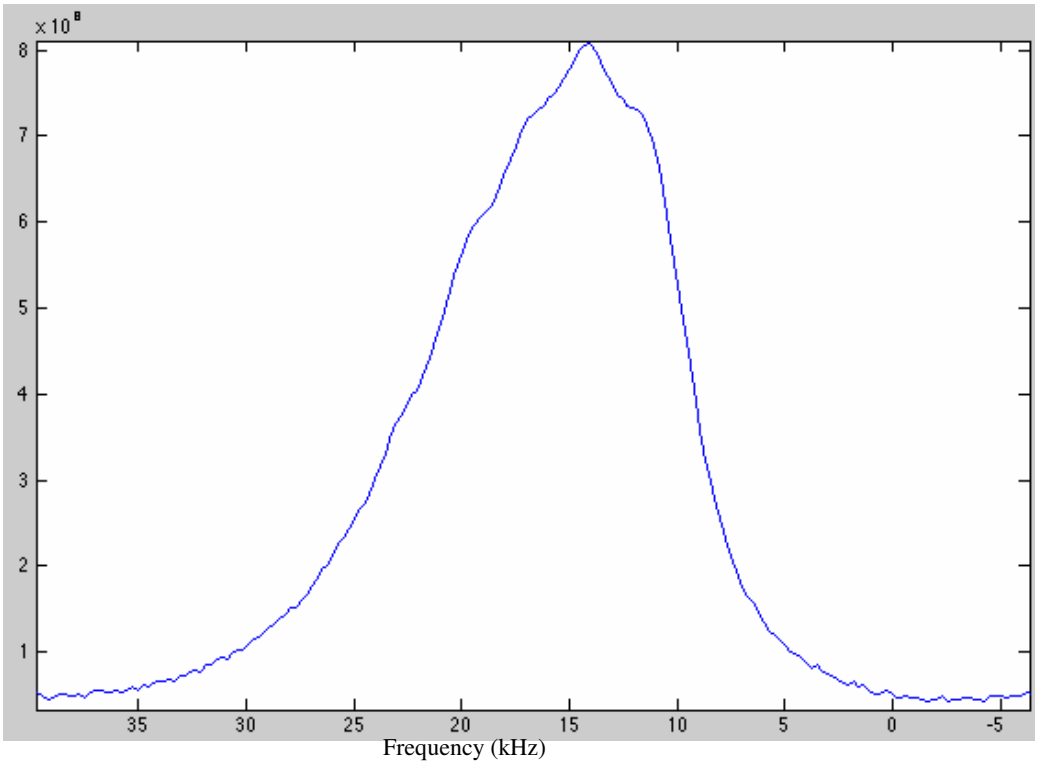

Fig 10: Center Band of fully relaxed PMSN at 230K, low resolution due to broad peaks

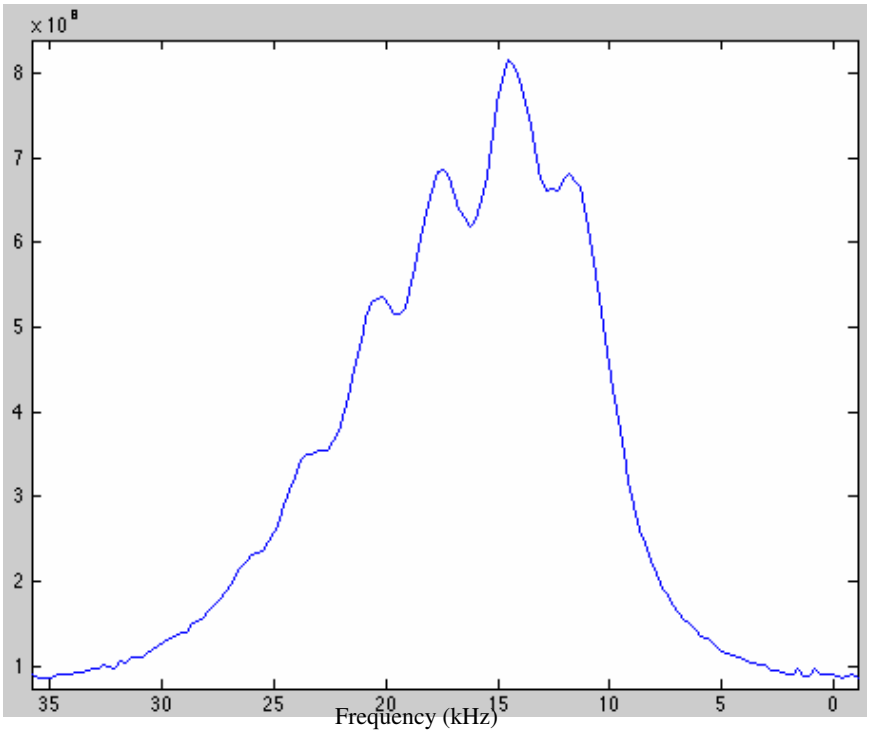

Fig 10a: Center band at T=270K. Note resolution of six peaks

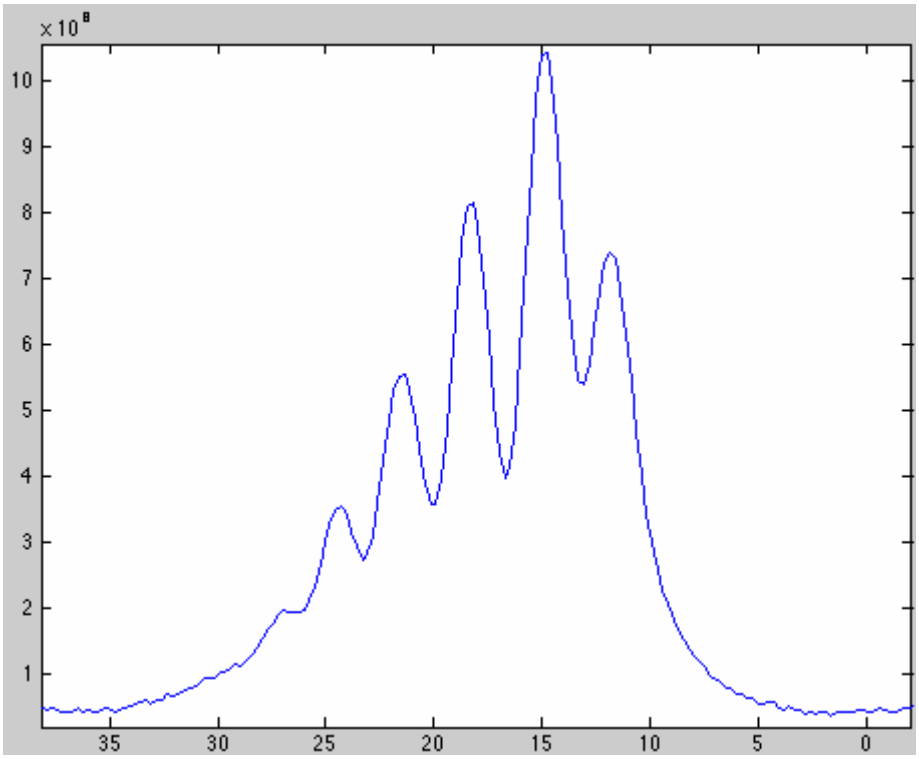

Fig 10b: center band at T=320K, highest temperature and greatest resolution

2.2.1 Frequency Shift Analysis

The frequencies of each peak are determined by the position of each respective ^{93}Nb nucleus in the lattice. Peak 0 for example is made up of all ^{93}Nb nuclei configured with six Sc^{3+} nuclei while peak 1 has five Sc^{3+} nuclei and one Mg^{2+} cations as the nearest B neighbors. The properties of the surrounding nBn nuclei and electrons cause an isotropic chemical shift (δ_{iso}^{CS}) in the resonant frequency of the ^{93}Nb nuclei. In addition to the isotropic chemical shift, since ^{93}Nb has a spin I =9/2, there is also a first and second order quadrupolar interaction which is in fact the more significant perturbation from the Zeeman Hamiltonian. The Hamiltonian follows equation 1 below.

$$H = H_Z + H_{iso}^{2Q} + H_{iso}^{CS} \quad \textbf{(1)}$$

Anisotropic perturbations, such as dipole-dipole and first order quadrupole, are removed with MAS. With these perturbations in mind, we examine the shifts in peak frequency over varying temperatures. Figure 11 shows a plot of the frequencies of the four largest peaks vs. set point temperature. As mentioned before, only the four largest peaks could be identified with significant certainty over the temperature range. The program used to exponentially fit the T_{1z} values did not allow a continuum of points; therefore there is an uncertainty of at least 0.488 kHz in each frequency. Lower intensity peaks (i.e. peak 4), uncertainty was larger due to difficulty in identifying the specific point of the peak, about 0.732 kHz as used in the plot.

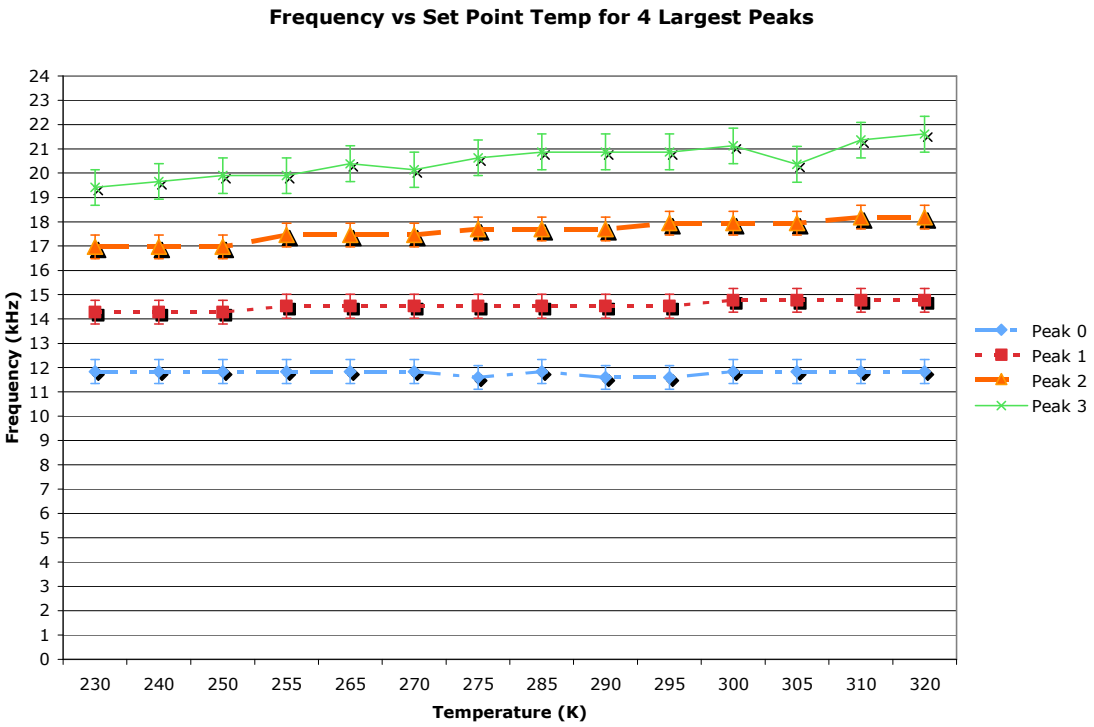

Fig 11: Frequency vs. Set Point Temperature for 4 Largest Peaks, showing minimal temperature dependence

It can be seen that in these four peaks there is very little shift in resonant frequencies with temperature. Peaks 0 and 1 have almost no change and are within experimental error, while peaks 2 and 3 shift at most by about 2 kHz over the span of 90 Kelvin. This implies that as the temperature varies, the static lattice properties (isotropic chemical shift and quadrupole interactions) change an almost insignificant amount.

2.2.2 T_{1z} Analysis

Using the variable delay before the final 90 degree pulse, we can see the overall relaxation of the ^{93}Nb nuclei to their original states. If there were no overlap in the peaks, individual configurations would be expected to have a purely single exponential decay to the fully relaxed state. The strength of the spectral lines is dependent on the *z*-component of the magnetization at a given time. The longer the delay, the more time the overall magnetization has to return to thermal equilibrium along the *z*-axis in line with the external magnetic field. Equation 2 shows the ideal form of the relaxation of the magnetization, assuming the initial magnetization is zero.

$$M_z(t) = M_{z,eq}(1-e^{-t/T_{1z}}) \qquad \textbf{(2)}$$

In equation 2, the time constant T_{1z} is the longitudinal relaxation time that we are interested in studying, while the variable t is the variable delay time used in the pulse sequence. For our fitting, a slightly more complex equation is used to account for small residual initial magnetization. For our shortest delay time (50 microseconds), there is a small bump in the center band that may possibly be from the D1 peak, which from previous studies has been shown to have significantly different parameters and therefore

a different (in this case much shorter) T_{1z} is seen. It is not until about 200 to 500 microseconds (in the 320K spectrum, longer at lower temperatures) that other peaks begin to take noticeable form. Figure 12 shows an exponential fit of peak 5 intensity at 320K, as well as a semilog fit. In the semilog plot, it is apparent that the exponential fit works very well with the data. On the other hand, figure 13 shows the semilog plot of peak 0, under which the distribution peak lies. The deviation from single exponential fit is much more significant here, with notable curvature, implying that there is likely a second peak of significantly different T_{1z} in the frequency that is being fit. This is expected, as previous studies have shown that the distribution peak behaves in a different manner than peaks 0-6. [2, 3, 4]

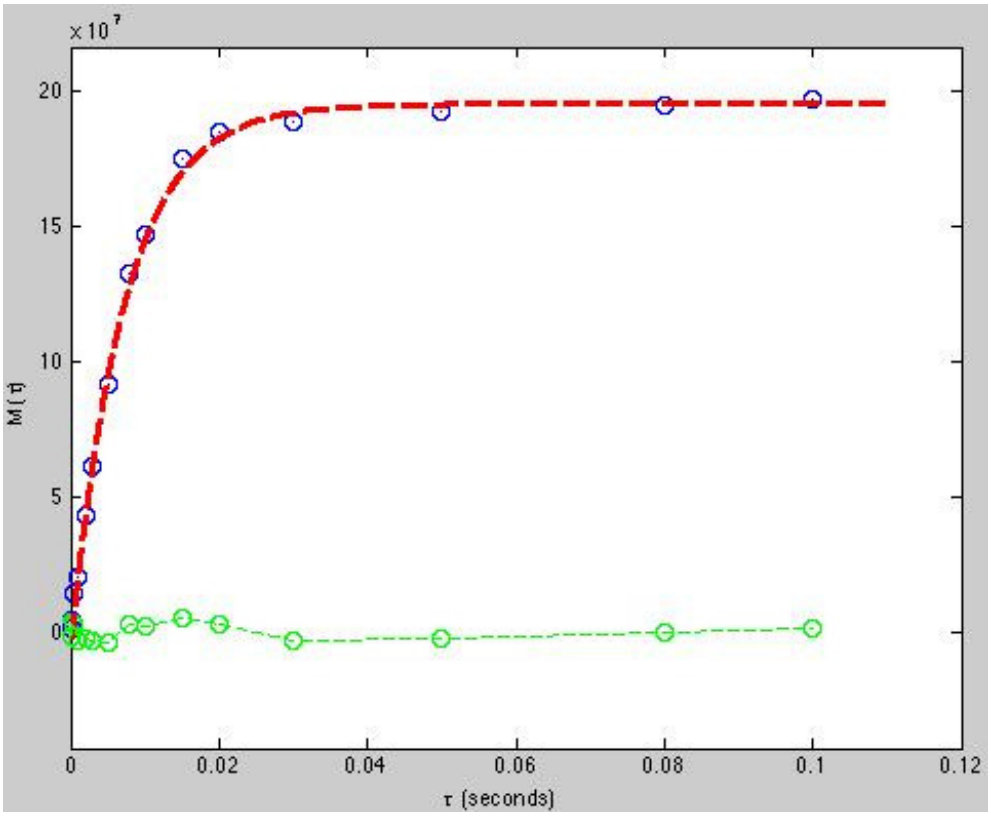

Fig 12: Exponential fit of peak 5 magnetizations, with green residuals on bottom showing deviation from exponential fit

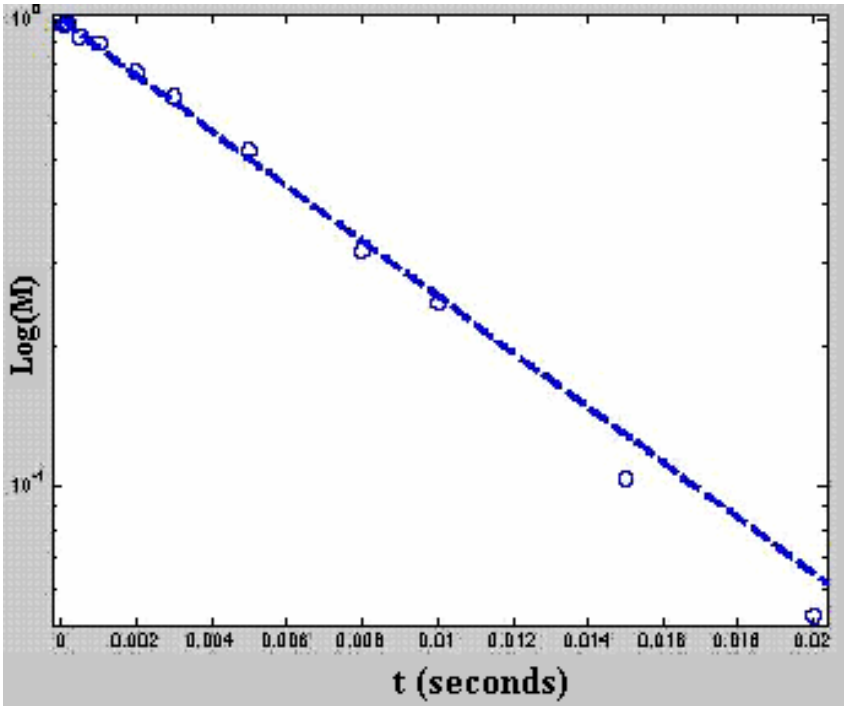

Fig 12a: Semilog fit of peak 5 magnetizations; note excellent linear fit

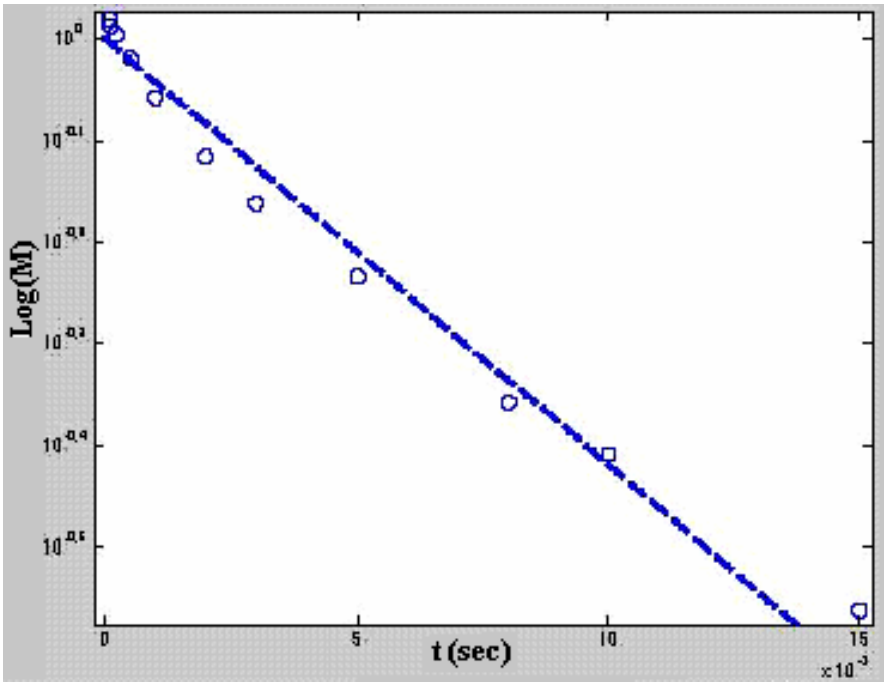

Fig 13: Semilog plot of peak 0 magnetization. Note the curvature of the fit implying biexponential behavior

We wish to examine the dependence of relaxation times on temperature. Figure 14 shows the plots of T_{1z} and R_{1z} vs. Temperature for the four largest peaks. R_{1z} is simply $1/T_{1z}$, and is what the fitting program outputs naturally. The R_{1z} plot includes error bars of 10%, based on the uncertainty given by the program when noise is taken into account. Not all peaks had the same uncertainty, but when noise was accounted for 10% was decided to be the best estimate to look for visual, qualitative comparison. Between the set point temperatures of 285-300 K, we see a very clear jump in R_{1z}, and this is the broad relaxor phase transition from the paraelectric to ferroelectric state. Outside of the transition range there appears to be some curvature, but much of it seems to be within experimental error. In addition, the R_{1z} values for separate peaks are very similar, mostly within experimental error other than possibly peak 3, which is still very close.

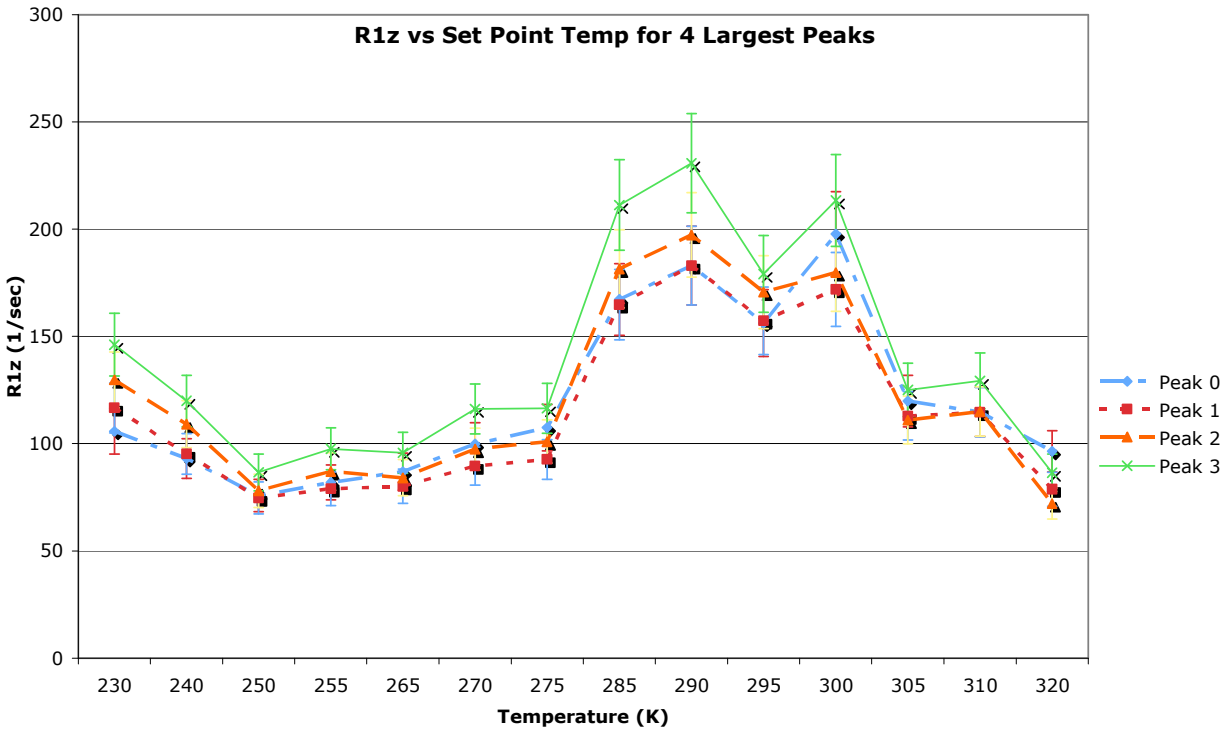

Fig 14: Plot of R_{1z} vs. T for 4 largest peaks showing strong temperature dependence

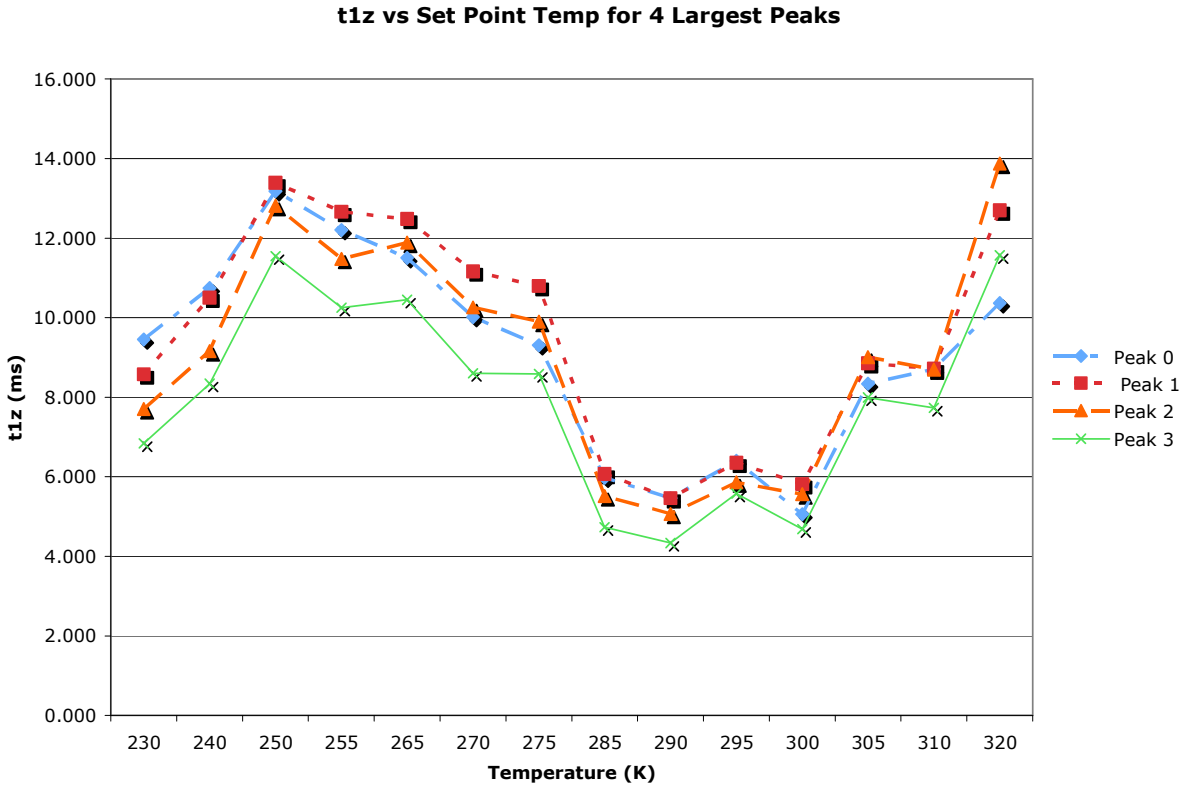

Fig 14a: Plot of T_{1z} vs T for 4 largest peaks with strong temperature dependence

2.2.3 Comparison of R_{1z} vs. Frequency Shift

The relaxation rate R_{1z} is primarily dependent on two factors: the motion of the ions within the crystal lattice, and the static properties of the lattice itself. The formula governing the rate is as follows:

$$R_{1z} = KC_q^2 f(\omega_0, \tau_c) \qquad \textbf{(3)}$$

In the equation, C_q is the quadrupole coupling constant which is determined by the electric field gradient created by the static orientation of the crystal sites. The function $f(\omega_0, \tau_c)$ is called the correlation function, and is dependent on the motions at the

Larmor frequency ω_0 and the correlation time τ_c, properties describing the motion of the system.[4]

According to previous theories, relaxor properties are thought to be primarily due to the structure of the crystals. However, by looking at the data presented in this study we see that the dynamics of the system play a very substantial role in the relaxor properties. By looking at the frequency shift over temperature, we see very little dependence on the temperature. Since the frequencies of the peaks show almost no change, then we can conclude that the quadrupole effects (quadrupole coupling constant and electric field gradient) produce a small or negligible change for these peaks. In contrast to the static frequencies, the relaxation rates show strong temperature dependence near the phase transition. With these two observations in conjunction with equation 3, we can see that the ionic motion (correlation function) plays an important role in the determination of the relaxation rates. Since the quadrupole constant is nearly constant for the peaks, the factor that most significantly influences the relaxation rate must be the dynamics.

3. Two Dimensional T_{1z} Analysis

After examining the one dimensional results, it was clear that there was overlap and interference between peaks, at the very least due to the distribution peak beneath the other peaks. As shown in figure 13, there is significant deviation from logarithmic decay, especially in peaks 0-3 under which the distribution peak primarily lies. Therefore we attempted to separate the peaks using Triple Quantum MAS (3QMAS), a two dimensional experiment that uses a series of RF pulses to excite triple quantum coherence instead of single quantum coherence as in the 1D experiments. The advantage of 3QMAS

is that it allows us to see more of what is hidden beneath larger peaks and examine individual peaks separately. The disadvantage of these experiments is that in order to excite triple quantum coherence, we need to force the forbidden transitions described previously. This causes severely reduced signal to noise ratio, and each experiment takes much longer. Whereas an entire set of 1D relaxation rate experiments for a given temperature may have taken approximately 2-3 hours, a single 3QMAS experiment (for just one delay in a relaxation series) takes anywhere from 2-5 hours to have usable data.[4]

3.1 Experimental Methods

We continued study with the exact same sample (in the same rotor) used in the 1D experiments. We initially used the mp3qzqf pulse program included in the Topspin II directory to set up and optimize pulse widths as an initial 3QMAS experiment without saturation-recovery. The pulse program contains an initial pulse to excite the system into the triple quantum coherence followed by another pulse of the same power but approximately ½ to 1/3 the width of the initial pulse to bring it back to single quantum coherence. There is then a selective 90 degree pulse to rotate magnetization into the acquisition dimension before digitizing and obtaining a FID. The pulse needed to be long and weak to excite only the center transition and remove spinning sidebands. An image of the pulse program is shown in figure 15 below**.** The final pulse values were 2.4 microseconds and 0.6 microseconds for P1 and P2, respectively, both at 0 dB, and 19 microseconds at 30 dB for P3, the selective 90 degree pulse. The delay between P1 and P2 was initially 1 microsecond and was incremented by 33.3 microseconds (equivalent to 1/30 kHz, the spinning frequency).

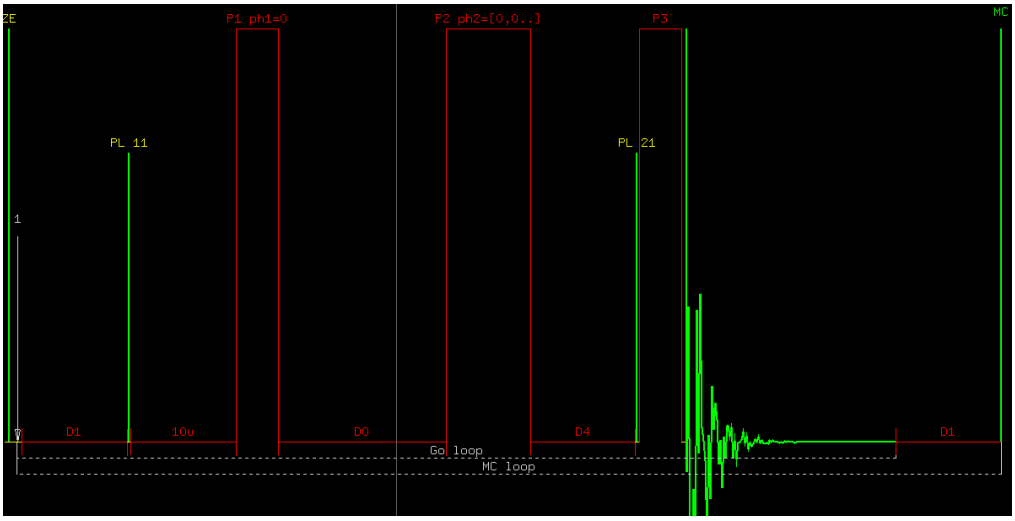

Fig 15: mp3qzf Pulse Program used for 3QMAS optimization with two pulses for 3Q excitation and one 90 degree acquisition pulse

Once the basic 3QMAS experiment was optimized, we used the optimal pulse lengths and powers but added a saturation pulse train identical to the train used in the 1D experiments, again 40 pulses of length of 1.6 microseconds at 3 dB. The pulse train was inserted before the 3Q excitation and after the pre-scan delay. After the pulse train, a variable delay D10 was added, which was modified to examine relaxation. By putting the pulse train before the 3Q coherence, we allow sites with different relaxation delays (supposedly the D1 sites) to evolve at their own rate, then show up more independently in the 2D spectrum. The pulse program is shown below.

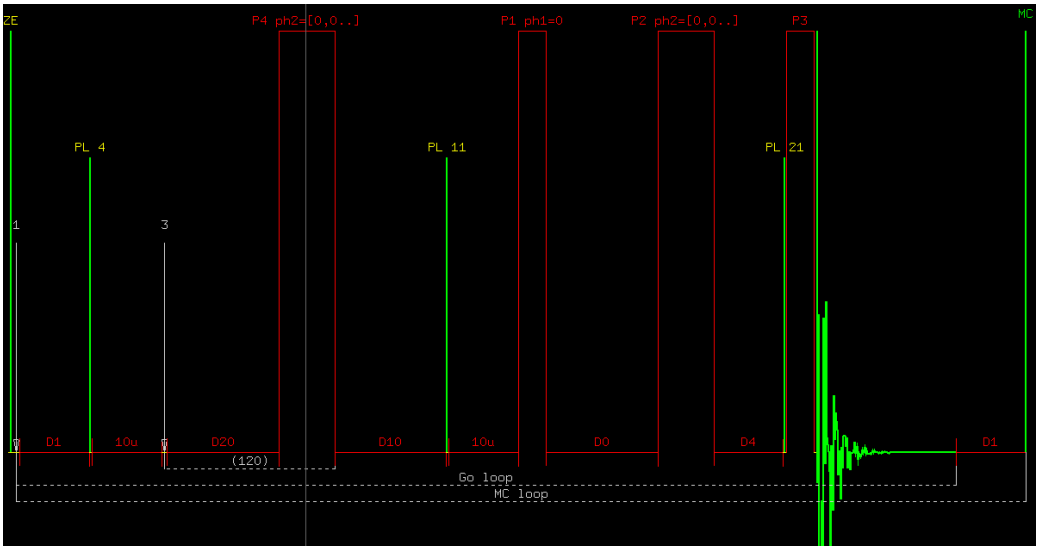

Fig 15a: 3QMAS experiment with Saturation Pulse train and previous 3QMAS pulses

In the early experiments, we initially ran into trouble with the program. The electronics in the spectrometer would not allow us to run experiments with short recovery delays, so we ended up needing to increase the pre-scan delay. With the electronics in the spectrometer, a recovery time of 30 microseconds was the shortest we felt comfortable using. If we made it any shorter, we ran the risk of burning out the probe due to too much high intensity RF radiation. Using the 30 microsecond delay, the shortest pre-scan delay we could run without failure was 50 milliseconds.

We ran 11 experiments with relaxation delays ranging from 30 microseconds to 100 milliseconds, at which the system was sufficiently relaxed to use as an infinity value. We focused on trying to get a significant number of shorter delays in an attempt to isolate the distribution peak. The experiments were run in this order of relaxation delay: 30μs, 10 ms, 75 ms, 50 μs, 250 μs, 5 ms, 100 μs, 2 ms, 1 ms, and 100 ms. Each experiment was run at 300K and used 4096 scans over 32 FID's of varying 3Q coherence.

3.2 Results and Analysis

When analyzing the 2D spectra, we noticed that one of the peaks, P0, that was prevalent in the 1D experiments, had essentially disappeared. This was evidently due to the symmetry of the site. Since P0 was defined by a niobium nucleus surrounded entirely by six scandium nBn's, the overall nature of the site is very symmetric. This decreased the quadrupole of the site to a point that no 3Q coherence could be excited in the 3QMAS experiment. Therefore, analysis we performed needed to be done without using the P0 peak.

In order to remove noise on the sides of the 2D spectra, we applied 500 Hz of exponential line broadening in the direct dimension F2 and 100 Hz in F1, the indirect dimension based on the 3Q evolution. This multiplies an exponential decay onto the FID, which prevents premature cutoffs that add sinc functions into the Fourier transform. Too much line broadening can distort the signal to a point that it may appear nice, but may actually be showing distorted data. Final processed 2D figures for a number of delays are shown below.

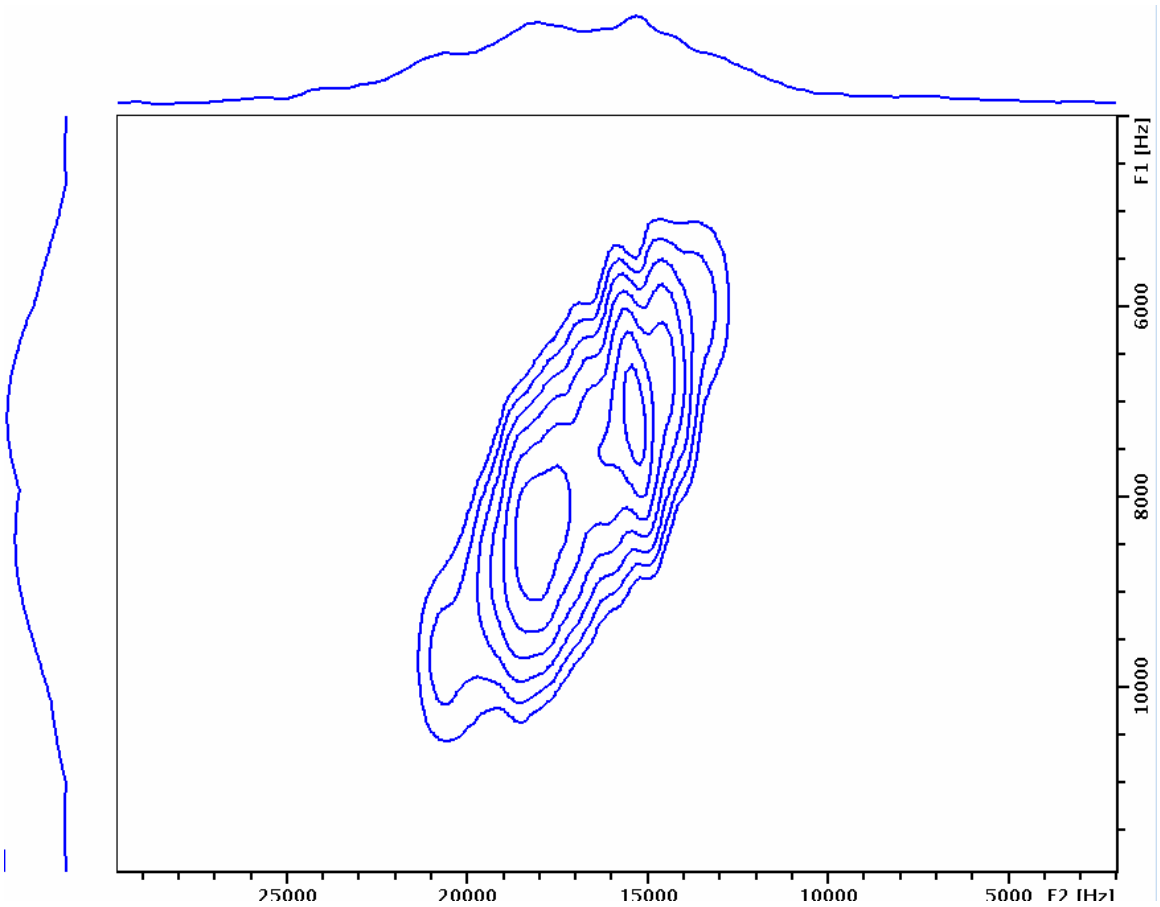

Fig 16: Fully relaxed (100 ms) spectrum at 300K

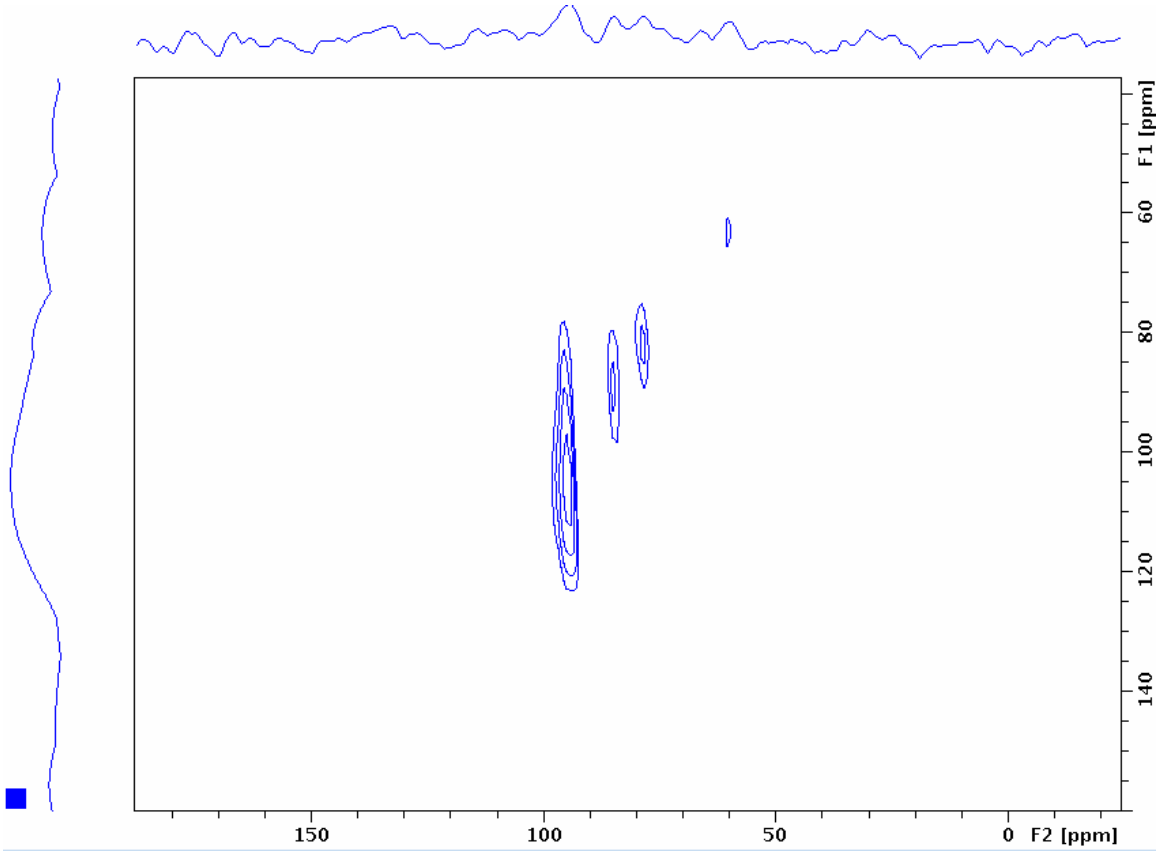

Fig 17: Spectrum of 30 microsecond delay at 300K

An additional experiment was performed with a higher number of scans to try to examine in more detail a 2D spectrum that was not fully relaxed. Figure 18 shows the spectrum at 250 microseconds, but run with 16 thousand scans instead of 4096 to improve signal.

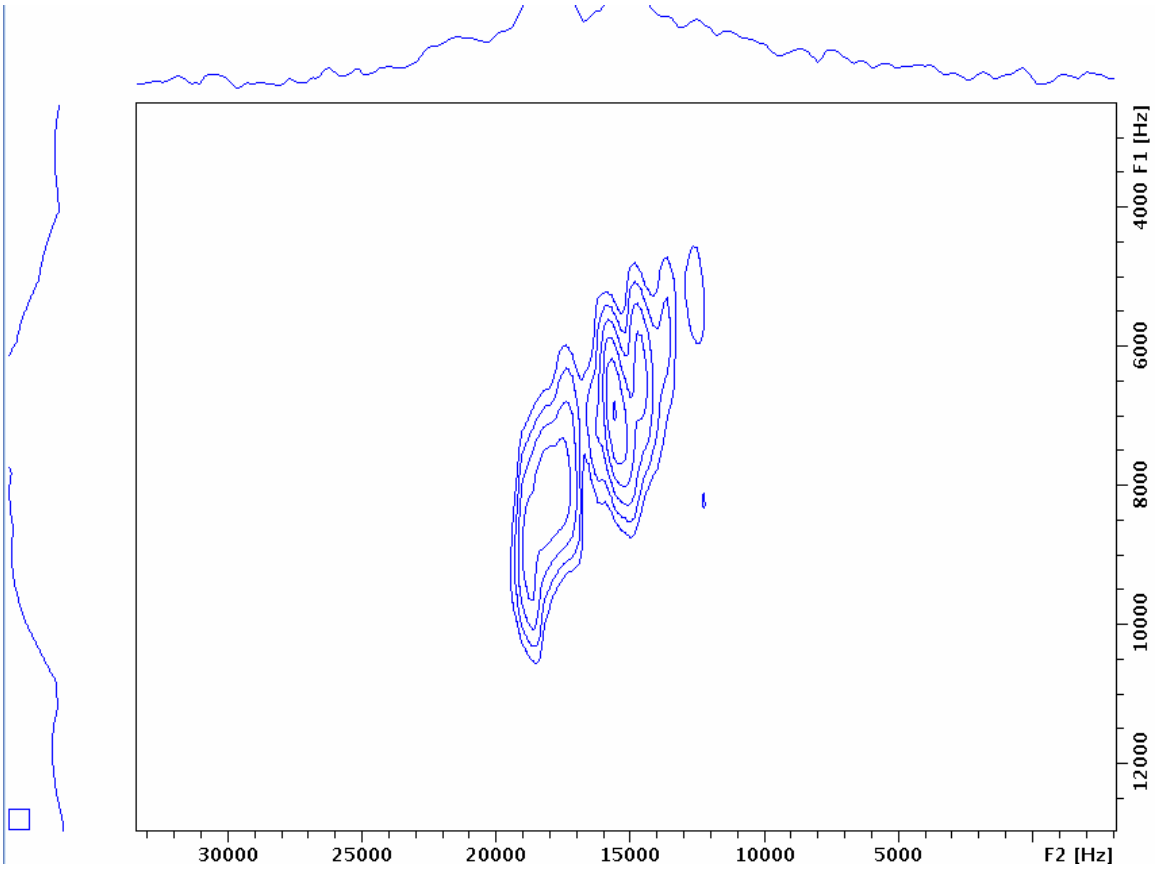

Fig 18: Spectrum of 250 microsecond delay with increased number of scans

3.2.1 Peak Deconvolution

In order to study the relaxation of individual peaks, we used ‘slices’ of the 2D spectra, in which we isolated a single frequency in the F1 dimension and examined the corresponding 1D spectrum in the F2 dimension. By examining the largest peaks in the fully relaxed spectrum, we saw that row 710 corresponded to P1 and row 669 corresponded to P2, with slight differences in frequencies from the 1D experiments due to distortion from the 3QMAS. The frequency for P1 in the 3QMAS experiments was 15.310 kHz opposed to 14.771 kHz in 1D, and P2 was shifted to 18.029 kHz opposed to 17.944 kHz in the previous experiments. Images of the relaxation evolution of the

individual slices are shown below, along with a superposition of the two slices to show the separation of the peaks. Other peaks were too small or broad to identify a slice using the data we obtained and the associated noise and low signal, so the analysis was performed only on the two largest peaks.

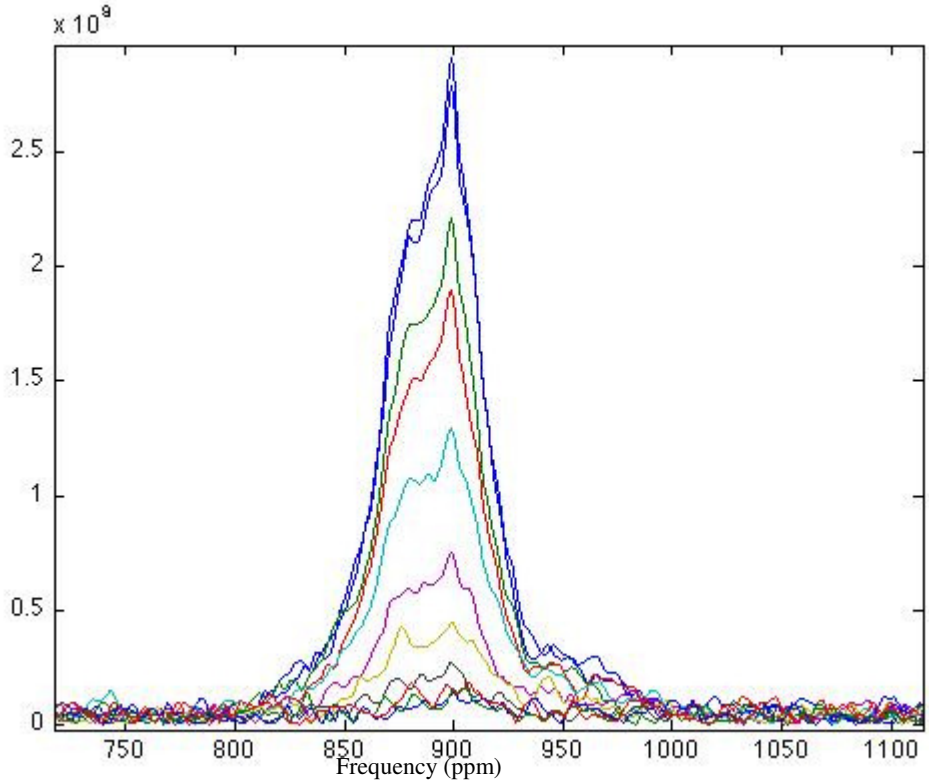

Fig 19: P1 slice recovery showing some remnant but reduced intensity of P2 and D1

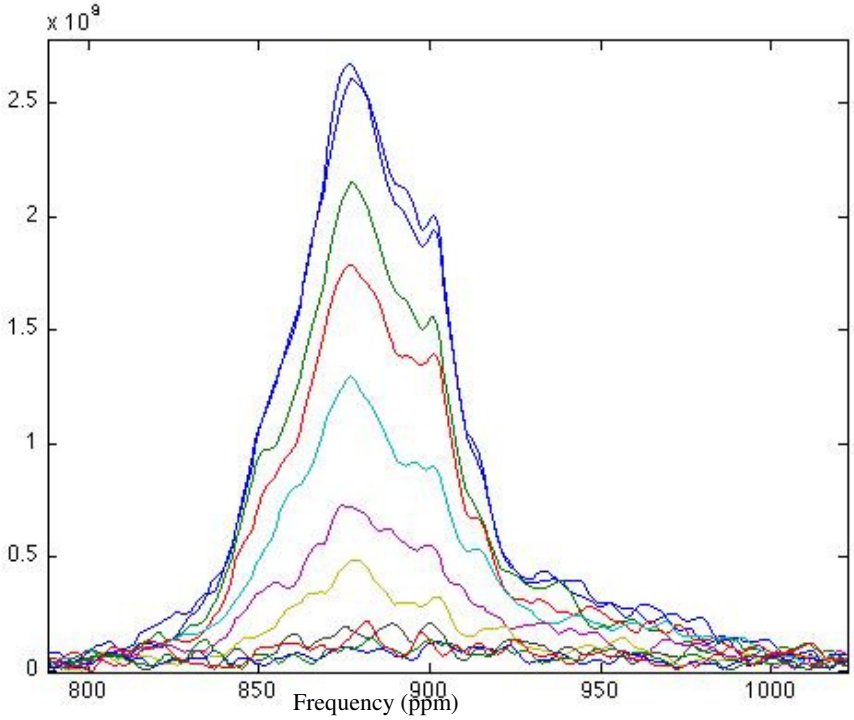

Fig 20: P2 slice recovery showing some remnant but reduced intensity of P2 and D1

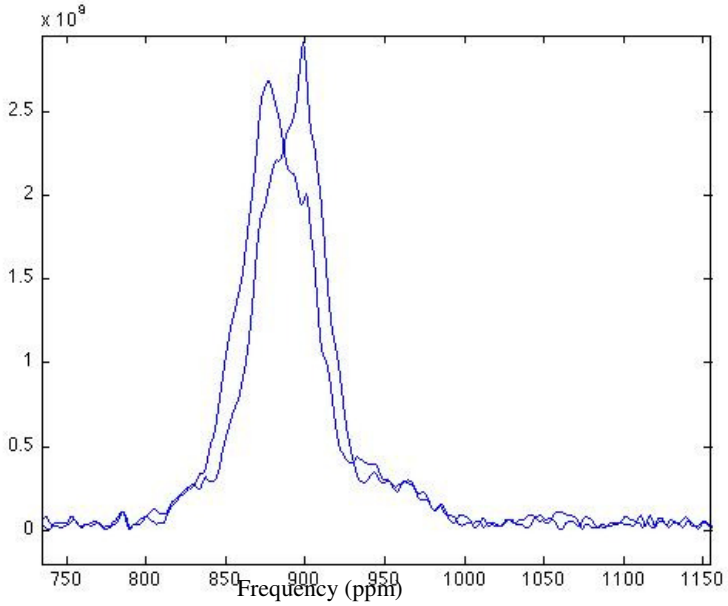

Fig 21: P1 (right) and P2 (left) superposition to show isolation of the peaks

There are a number of traits to notice in the superposition figure. First, note the shoulder that appears to be a broader peak beneath the two sharper peaks P1 and P2. This is what we expected to be the D1 peak with significantly different relaxation values. It is still beneath the other peaks, as we were unable to completely separate it into an independent slice for more precise analysis.

Second, it is apparent that there is still some overlap between peaks P1 and P2, but they are partially resolved. The larger peak P1 is significantly reduced in the P2 slice, as is the P2 intensity in the P1 slice, showing that the deconvolution is not quite complete, but acceptable.

3.2.2 Relaxation Fitting

With the two largest peaks separated, we were able to fit them to relaxation curves using a MATLAB script. The script allowed us to take a number of points on each slice, then at that specified frequency on each recovery curve, it fit the magnetization to an exponential curve using the 100 ms slice as an infinity value to scale in comparison with. Points selected for fit are shown in figure 22, along with semilog plots for significant points.

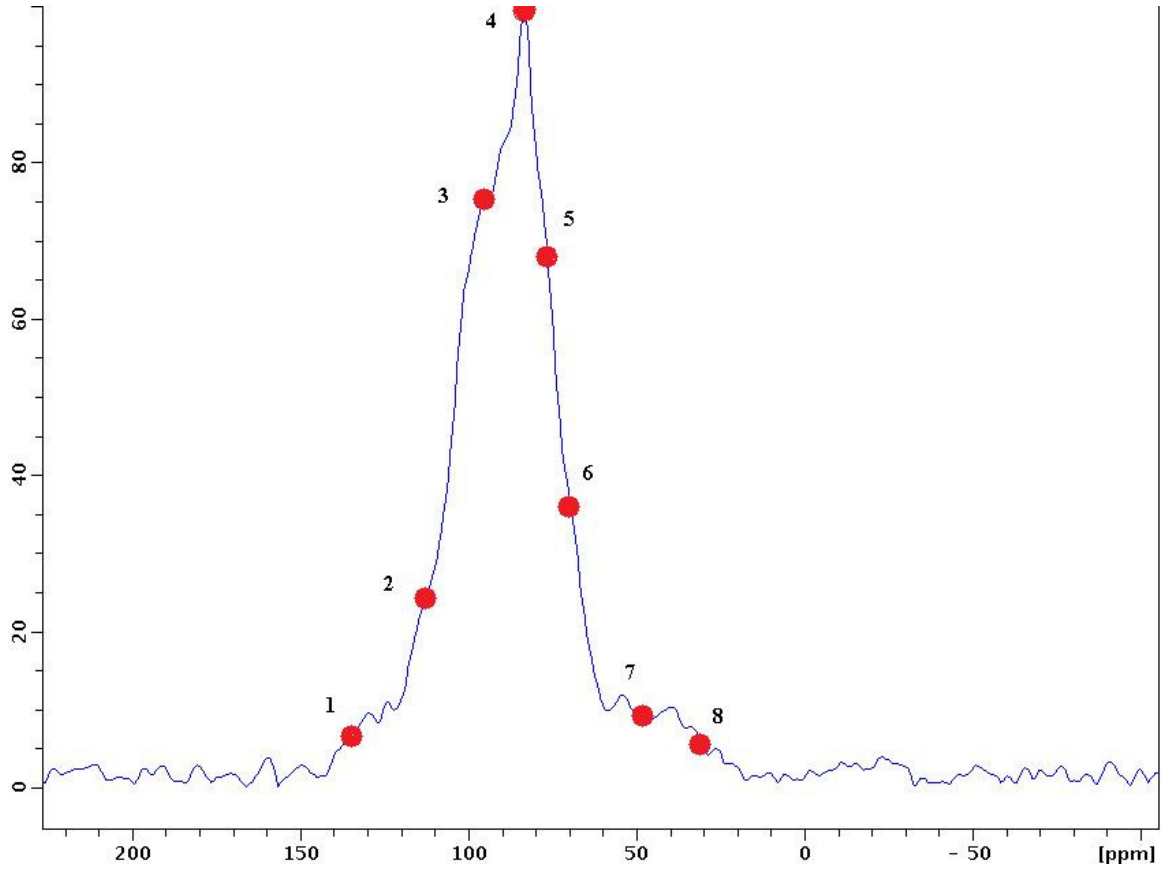

Fig 22: Peak 1 Selected Points

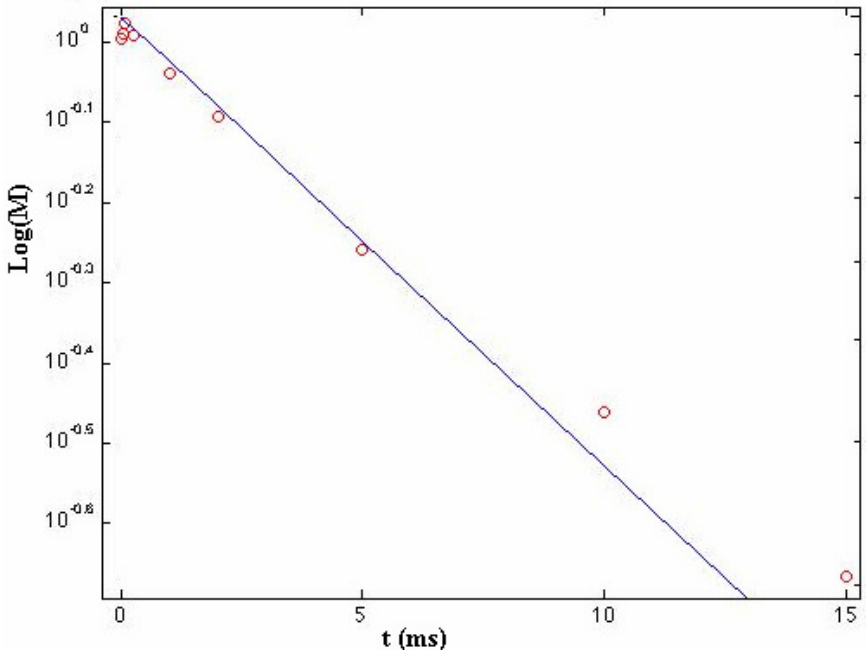

Fig 23: Peak 1 Point 3 Semilog Recovery Fit showing near linearity due to spin diffusion

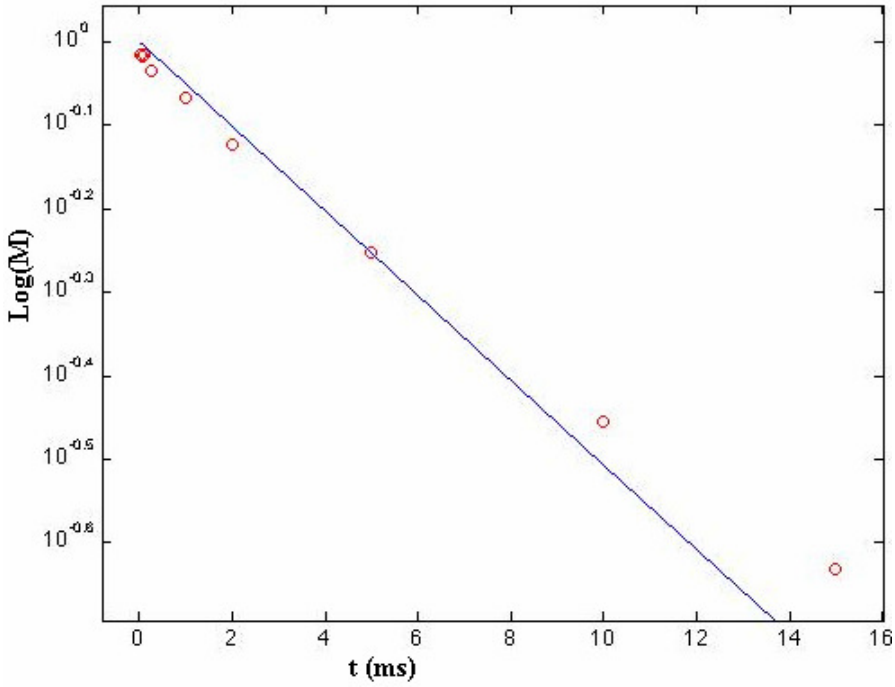

Fig 24: Peak 1 Point 4 Semilog Recovery Fit with some biexponential curvature

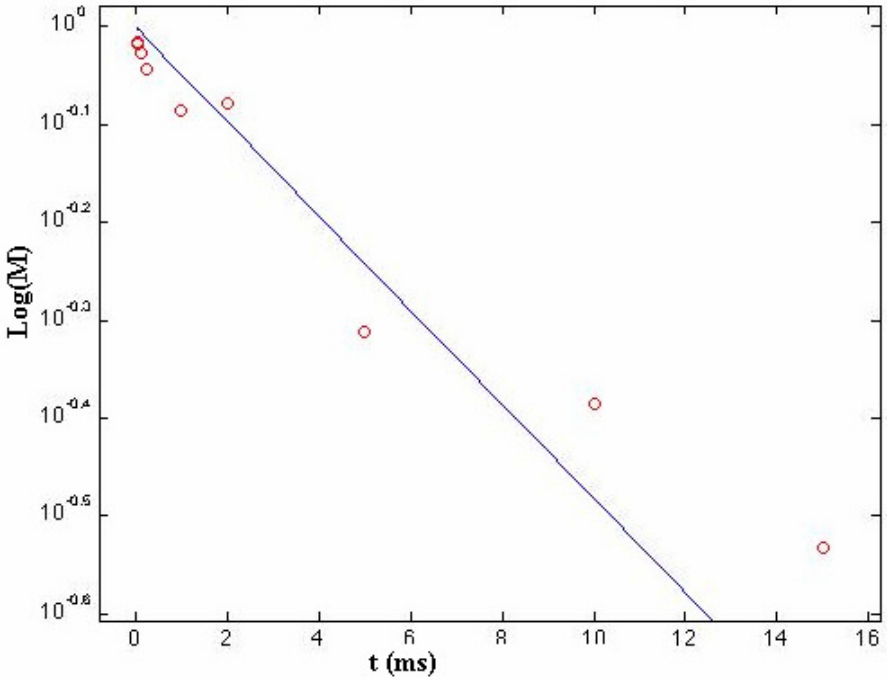

Fig 25: Peak 1 Point 6 Semilog Recovery Fit with strong biexponential curvature from D1 influence

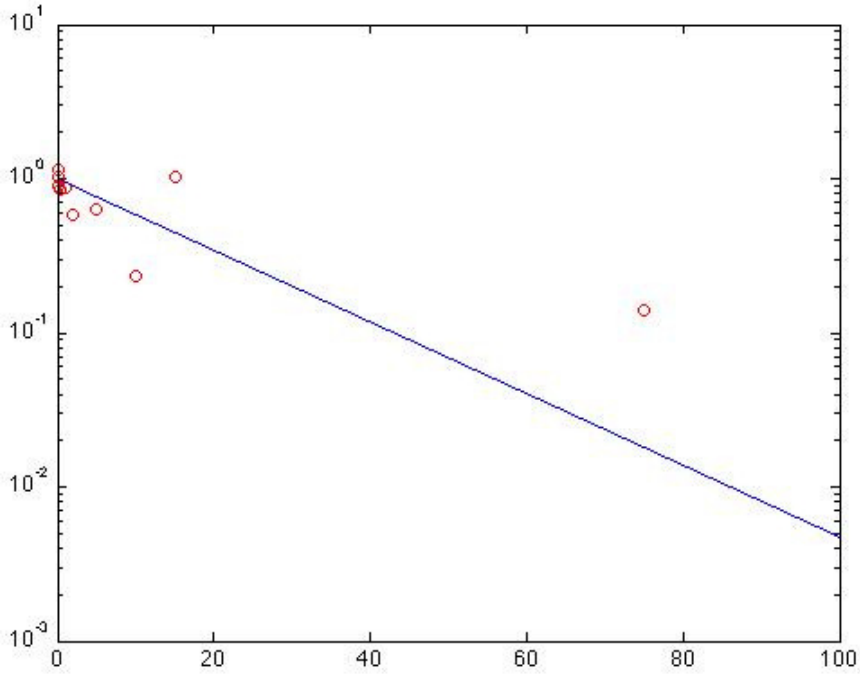

Fig 26: Peak 1 Point 8 Semilog Recovery Fit (no significant fit)

Figure 26 is displayed to show how much noise interfered with the fit, especially at lower points in the spectrum. We had hoped to examine the relaxation rate of the shoulder on the edge of the peak to see the behavior of the D1 peak, but the noise associated with the 3QMAS experiment prevents us from achieving reliable data at such low points. Looking at the other figures, we can notice some slight curvature in the fit indicating biexponential decay. Point 3 has the least curvature of all points examined, even though it is the point where P2 is at a maximum in its own slice. This is an expected consequence of cross relaxation (spin diffusion due to unresolved dipole couplings). Point 4 is where P1 is at a maximum but the curvature of the fit shows that there is still an additional influence of a separate peak, likely the D1 seen at the bottom, as well as the suppression of the cross relaxation seen in point 3. Point 6 shows the most extreme curvature, which fits our expectation that since the difference between P1 and D1 at that point is the smallest there (among points not overwhelmed by noise), so D1 would have the greatest influence there. We processed the slice for P2 in the same manner, shown in the figures below.

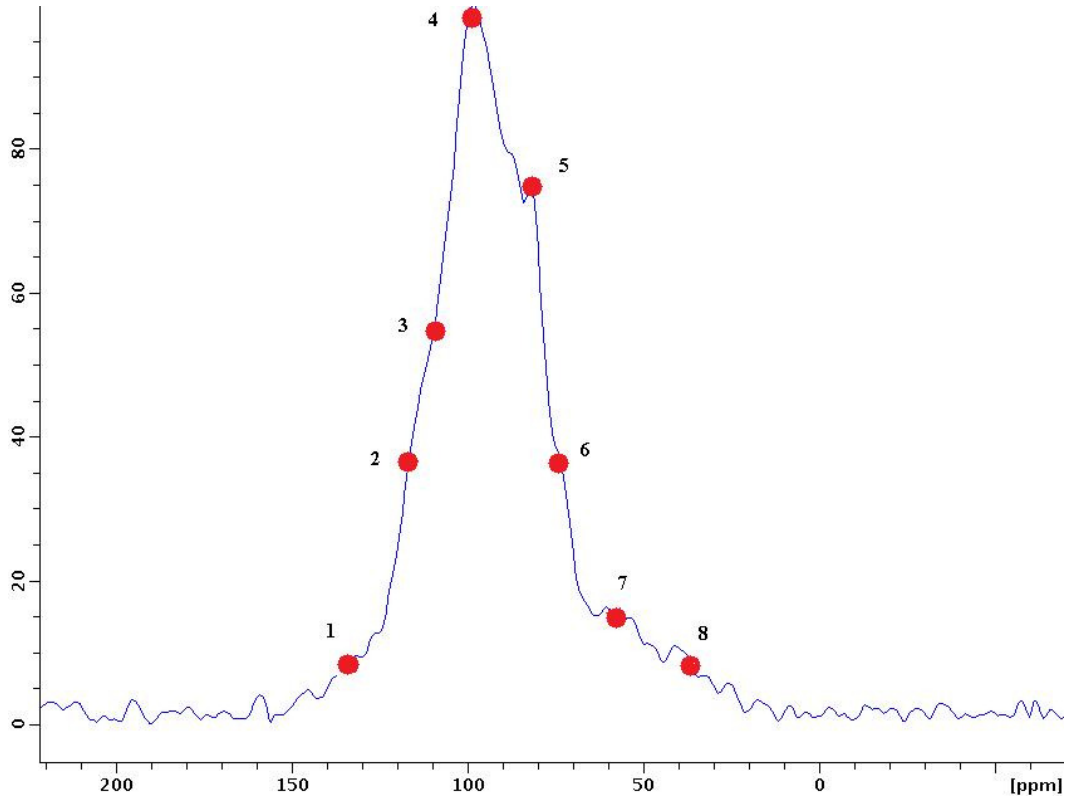

Fig 27: Peak 2 Selected Points

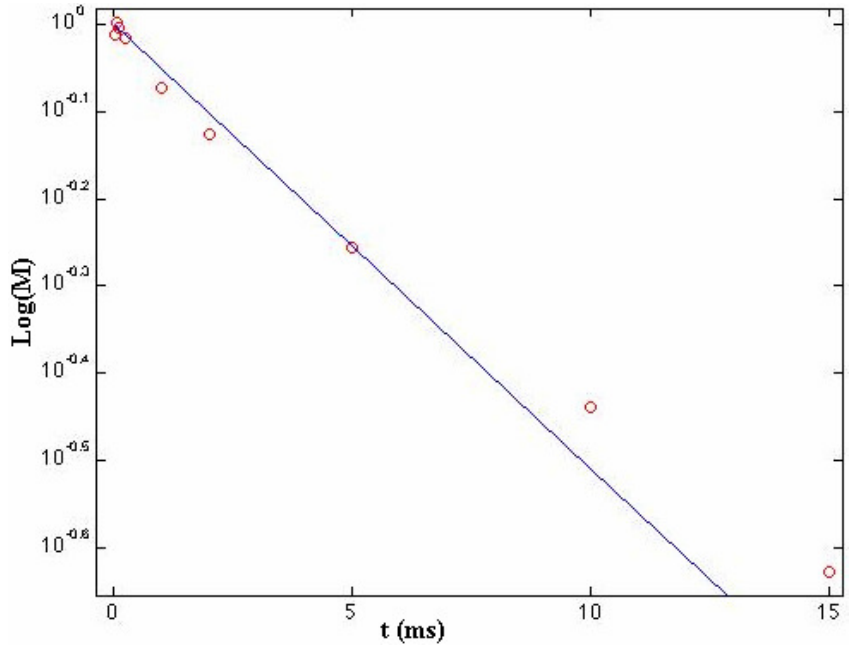

Fig 28: Peak 2 Point 3 Semilog Recovery Fit showing slight biexponential curvature

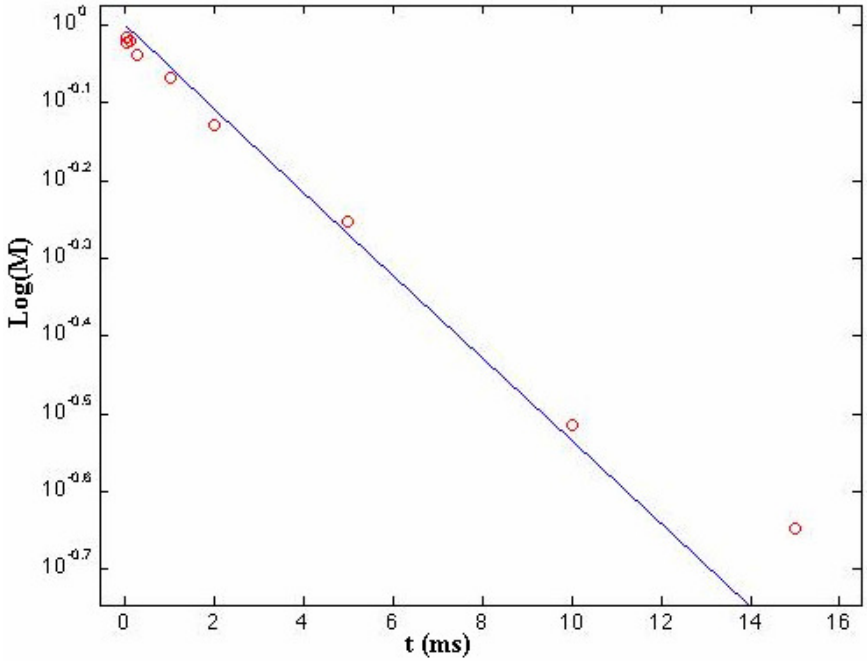

Fig 29: Peak 2 Point 5 Semilog Recovery Fit with near linear fit from spin diffusion

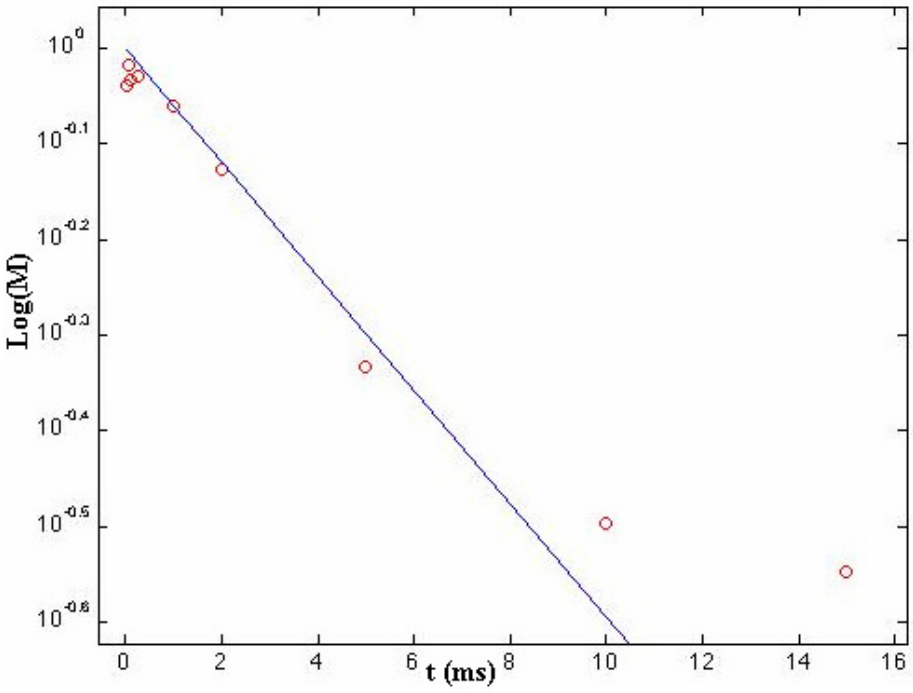

Fig 30: Peak 2 Point 6 Semilog Recovery Fit showing strong biexponential curvature from D1 influence

Again we see that in Point 6 (close to the D1 peak), there is significant curvature, though points 3 and 5 appear to fit the recovery curve very well. In looking at the curves, we can generally see that the trend of points crosses over the line of exponential fit between 6-10 milliseconds, showing that there is a much faster process that dies out sometime around then, likely the D1 peak decay.

3.2.3 T_{1z} Values

For points described above, the table below shows their respective R_{1z} relaxation rates, T_{1z} longitudinal relaxation times, and a brief note of how well they fit the semilog exponential.

Peak Number	Point Number	R_{1z} (1/ms)	T_{1z} (ms)	Degree of Fit
1	1	0.0997	10.030	unusable
1	2	0.1355	7.380	unusable
1	3	0.1271	7.868	acceptable
1	4	0.1164	8.591	acceptable
1	5	0.1091	9.166	acceptable
1	6	0.1111	9.001	strong double exponential
1	7	0.1914	5.225	unusable
1	8	0.0536	18.657	unusable
2	1	0.0925	10.811	unusable
2	2	0.1213	8.244	unusable
2	3	0.1172	8.532	acceptable
2	4	0.1266	7.899	acceptable
2	5	0.1231	8.123	acceptable
2	6	0.1369	7.305	some double exponential
2	7	0.1789	5.590	strong double exponential
2	8	0.2206	4.533	unusable

Fig 31: Table of R_{1z} and T_{1z} for points taken showing increase T_{1z} values

In both peaks, we see that the T_{1z} is shorter as we go further to the right of the spectra, where the D1 peak is more prevalent. Indeed, as the double exponential evidence increases, the relaxation time decreases. This is evidence of the fact that the D1 does behave in a manner different from the other peaks in the system.

To define the peaks, we shall use the point numbers at which each peak is greatest. For both peaks, this is point 4. If we compare the T_{1z} values shown here to the T_{1z} values at 300K in the 1D studies, shown below, we see that there is a definite increase in relaxation time after the analysis of 3QMAS data.

Temp	Peak 0 T1z	Peak 1 T1z	Peak 2 T1z	Peak 3 T1z	Peak 4 T1z	Peak 5 T1z
230	9.455	8.571	7.705	6.844		
240	10.747	10.501	9.163	8.339	7.154	
250	13.186	13.391	12.810	11.545	10.723	
255	12.207	12.663	11.483	10.247	8.783	
265	11.504	12.482	11.888	10.447	9.036	
270	10.014	11.162	10.261	8.604	6.314	4.786
275	9.307	10.795	9.901	8.582	6.889	5.943
285	5.979	6.068	5.511	4.734	4.076	3.346
290	5.464	5.464	5.069	4.334	3.494	2.813
295	6.399	6.354	5.862	5.581	4.989	4.483
300	5.057	5.817	5.564	4.687	3.76	2.997
305	8.34	8.854	9.010	7.995	7.295	6.529
310	8.71	8.719	8.695	7.734	6.59	5.272
320	10.368	12.695	13.874	11.569	9.82	7.303

Fig 32: Table of T_{1z} values for peaks from 1D analysis for comparison. At 300K, T_{1z} values are significantly shorter than those found in 3QMAS study

This increased relaxation time shows us that though the D1 peak has not been completely removed from the other peaks, it has been removed to a significant extent from the other peaks that it lies beneath in 1D spectra.

4. Conclusions

In the 1D experiments, frequency shift analysis shows that there is very little influence of temperature on the resonant frequency of the four largest peaks. However, there is a definite significant temperature dependence of the relaxation rates for each peak, and since the quadrupole and chemical shifts seem to remain constant we conclude that the dynamics of the ions in the lattice account for much of the relaxor behavior in the PMSN system. Due to the complex structure of the unit cells, it is logical to assume that there is at least one phonon mode that runs through many units in conjunction to create the lasting macroscopic polarization unique to relaxor ferroelectric materials. Previous studies have shown that the nBn structure can have a drastic impact on the positions of the oxygen lattice in a single unit cell, and with many possible phonon modes these oxygen displacements likely have a significant impact on the remnant polarization.

From the 2D experiments, we further saw that there was a significant impact in the spectral analysis from the D1 distribution peak resting beneath the other peaks. However, its effect was removed to a certain extent through the deconvolution process. By separating the peaks with 3QMAS experiment and analysis, we were able to see a more accurate depiction of the relaxation rates of specific nBn sites. Though the deconvolution was not complete, we have shown that more advanced and in-depth 3QMAS experiments can allow us to isolate and study specific sites separately. In the future, experiments can be performed over longer periods to further separate peaks and look more closely at the D1 distribution peak.

References

[1] R. L. Vold, G. L. Hoatson, M. Vijayakumar, Variable temperature ^{93}Nb NMR investigation of local structure and polar nanoclusters in lead magnesium niobate/lead scandium niobate solid solutions, Physical Review B75 (2007) 134105-1-9

[2] D. H. Zhou, G. L. Hoatson, R. L. Vold, Local structure in perovskite relaxor ferroelectrics: high-resolution ^{93}Nb 3QMAS NMR, Journal of Magnetic Resonance 167 (2004) 242-252

[3] D. H. Zhou, Multinuclear NMR studies of Relaxor Ferroelectrics, PhD thesis

[4] M. J. Duer, Introduction to Solid State NMR Spectroscopy

[5] D. J. Griffiths, Introduction to Quantum Mechanics (Second Edition)

I would also like to thank Dr. Gina Hoatson and Dr. Bob Vold for all the help that they have given me in learning to run these experiments, and even more for helping me understand more advanced details. Additional thanks to grad students Chris Maher and Jeremy Ellden, who helped me become familiar with the spectrometer and offered additional advice.

Appendix: MATLAB scripts used

```
% script to extract recovery curves from slices of 3QMAS
spectra
%
% function get_recovery_curves
clear % start with a clean workspace

load slices_710_669.mat  % this is the workspace saved after
running the slice extraction script
%
% make a frequency axis for use in plotting the slices
%
sw = 250; % kHz -- edit this to match spectral window in F2
npts = size(slices{1},1); % points in slice

spectrum_limit=(sw/2)*(1-1/npts); %Calculate the left and
right limits of the spectrum with one scalar
ax = linspace(-spectrum_limit,spectrum_limit,npts)'; %
frequency axis for spectral plotting; zero at center
%
% plot last spectrum (assumed to be the infinity value)
%
nslice = size(slices,1); % number of slices
rcf = cell(size(slices)); % space for recovery curves, one
set for each slice
for ns = 1:nslice  % loop over slices
    %
    % expand region
    %
    figure(1) ; hold off ;
    spec = slices{ns}(:,end); % use the infinity spectrum
    base = zeros(ntau,1); % space for base line values
    plot(spec)
    [x,y] = ginput(2);
    lower = fix(x(1)); upper = fix(x(2));
    fax = ax(lower:upper);
    tmp = spec(lower:upper);
    plot(tmp)
    [x,y] = ginput(2); % select a region free of peaks to
define the baseline
    blpts = fix(x);  % x(1) is left point number of baseline,
x(2) is right edge point number
    hold on
    plot((blpts(1):blpts(2))',tmp(blpts(1):blpts(2)),'r')
    base(end) = mean(tmp(blpts(1):blpts(2))) ; % baseline
for infinity spectrum
    [x,y] = ginput ; % select an arbitrary number of points
on the infinity spectrum
    nps = length(x) ; % nps is the number of points selected
    rc = zeros(ntau,nps); % space for recovery curves of
current slice
```

```
    rc(end,(1:nps)) = y-base(end) ; % baseline-corrected
infinity values for each point
    for kk = 1:ntau-1
        tmp = slices{ns}((lower:upper),kk);
        base(kk) = mean(tmp(blpts(1):blpts(2))); % base line
for current tau-value
        rc(kk,(1:nps)) = tmp(fix(x))-base(kk); % baseline-
corrected points for curent tau-value
    end
    rcf{ns} = rc;
end
figure(2)
semilogy(tvals,rc(:,1+fix(nps/2)))
```

```
% script to read a processed Topspin file
clear
%
% enter relaxation delays
%
tvals = inputdlg('enter relaxation delays');
tvals = str2num(tvals{1})';
ntau = length(tvals); % number of relaxation delays
tvals = sort(tvals); % sort into increasing order
%
% enter slice numbers
%
slice_numbers = inputdlg('Enter row numbers( for F1) of
slices along F2: ');
slicenums = str2num(slice_numbers{1})';
nslice = length(slicenums);
%
% read the infinity spectrum: each ROW will be a FID along
F2
%
[filename, pathname] = uigetfile('*.*', 'Select the infinity
file (processed 2D only!');
datatype = 'complex';
[tmpdata, ndim, n] = read_proc(pathname, datatype);
tmpdata = tmpdata';
%
% reserve space for slices: one cell for each peak, contains
a nxm array of
% zeroes ,where n = fid length, and m = number of relaxation
delays
% Put infinity slices into the last columns of each array
slices = cell(nslice,1);
for jj = 1:nslice
    slices{jj} = zeros(size(tmpdata,2),ntau);
    slices{jj}(:,ntau) = real(tmpdata(slicenums(jj),:));
end
%
% read the rest of the 2D data files, one for each data set,
extract & store slices
% (this overwrites tmpdata array)
%
%
% NOTE: THIS MUST BE DONE IN INCREASING ORDER OF RELAXATION
DELAY!!
%
for jj = 1:(ntau-1)
    [filename, pathname] = uigetfile('*.*', 'Select the
infinity file (processed 2D only!');
    datatype = 'complex';
    [tmpdata, ndim, n] = read_proc(pathname, datatype);
    tmpdata = tmpdata';
    for kk = 1:nslice
```

```
    slices{kk}(:,jj) = real(tmpdata(slicenums(kk),:));
end
end
```

```
function [mzero,minf,R1Z] =
R1Zfit(data,mask,figcount,jjj,kkk)
%
% [mzero,minf,T1Z] = R1Zfit(data) does non-linear least
squares
%                                   fit of a recovery curve to
a single
%                                   exponential.
%
% data(:,1) is the list of tau values, data(:,2) are the
corresponding m(tau)
%
%       mzero is the best-fit magnetization at tau = 0,
%       minf is the best fit magnetization at tau = infinity,
%       R1Z=1/T1Z is the best fit relaxation RATE;
%       T1Z = 1/R1Z in the same units as delay times tau.
%

% construct tau-list and recovery curve, omitting masked
points
nmax = size(data,1);  % length of full tau list
tau = zeros(nmax,1);
fdata = zeros(nmax,1);
kk = 1;
for jj = 1:nmax
    if mask(jj) ~= 0
        fdata(kk) = data(jj,2);
        tau(kk) = data(jj,1);
        kk = kk + 1;
    end
end
tau = tau(1:(kk-1)); fdata = fdata(1:(kk-1));
last = length(tau);
minf = fdata(last); % assume last point is a good infinity
value
fm = 1-fdata/minf ; % normalized recovery curve, for
plotting purposes only
m_zero = 0;
r1z_zero = 1/tau(fix(length(tau)/2));
dcor = fdata;
pz = [r1z_zero m_zero minf]; % initial guesses, needed to
start iterations
%dcor = fdata;
pfit = fminsearch(@(pfit) t1ir(pfit,tau,fdata),pz); %
simplex fit routine
dd = pfit(3) + (pfit(2)-pfit(3))*exp(-pfit(1)*tau);
fd = (1-dd/pfit(3));
figure(figcount);
str = sprintf('%s%d%s%d','Peak Number',jjj,'point
number',kkk);
        set(figcount,'Numbertitle','off','Name',str)
semilogy(tau,fm,'ro',tau,fd,'b-'); % semilog display of
fitted curve
mzero = pfit(2);
```

```
R1Z = pfit(1);
minf = pfit(3);
function sumsq = t1ir(x,tau,data)
%
% x(3) = m(inf) ; x(2) = m(0) ; x(1) = 1/T1Z
% This one is for 3-parameter, single exponential do_glfit
to T1 or T2 data
sim = x(3)+(x(2)-x(3))*exp(-x(1)*tau) ;
dev = sim(:)' - data(:)' ;
sumsq = sum(dev.*dev);
```

```
% script to plot (M(inf)-M(tau))/M(inf)
%
% rcf{1} holds an array rc(:,1:nps) of recovery curves for
first peak
% rcf{2} holds an array rc(:,1:nps) of recovery curves for
second peak
%
figcount = 1;
t1data = cell(size(rcf));
for jj = 1:nslice % loop  over slices
    Rcurves = rcf{jj};
    M = zeros(size(Rcurves));
    npeaks = size(Rcurves,2);
     t1data{jj} = zeros(npeaks,3);
    for kk = 1:npeaks % loop over recovery curves for
current slice
%         M(:,kk) = 1-Rcurves(:,kk)/Rcurves(end,kk);
          data = [tvals Rcurves(:,kk)];
          [mzero,minf,R1Z] =
R1Zfit(data,mask,figcount,jj,kk);
          t1data{jj}(kk,1) = mzero ;
          t1data{jj}(kk,2) = minf;
          t1data{jj}(kk,3) = R1Z;
          figcount = figcount+1;
    end
%     R = M((1:ntau-1),:);
%     for kk = 1:(npeaks-1)
%         figure(figcount)
%       str = sprintf('%s%d%s%d','Peak Number',jj,'point
number',kk);
%       set(figcount,'Numbertitle','off','Name',str)
%       plot(tvals(1:(ntau-1)),log(R(:,kk)));
%       pos = get(figcount,'position');
%       pos(1) = pos(1) + 10; pos(2) = pos(2)+10;
%       set(figcount,'position',pos)
%       figcount = figcount+1;
%     end
% end
```